Do Specific Ion Effects on Collective Relaxation Arise from Perturbation of Hydrogen-Bonding Network Structure?

Jennifer A. Clark[†,*] *and Jack F. Douglas*[†,*]

[†]Materials Science and Engineering Division, Material Measurement Laboratory, National Institute of Standards and Technology, 100 Bureau Drive, Gaithersburg, Maryland 20899

Keywords: monatomic ions, Hofmeister series, chaotropic ion, kosmotropic ion, hydration layer, Debye-Waller parameter, neutron scattering, collective intermediate scattering function, collective relaxation time of water, viscosity *B* coefficient, shear viscosity, water diffusion coefficient.

*Corresponding authors: jennifer.clark@nist.gov; jack.douglas@nist.gov

Abstract

The change in the transport properties (i.e., water diffusivity / shear viscosity) when adding salts to water has been used to classify ions as either being *chaotropic* or *kosmotropic*, a terminology based on the presumption that this phenomenon arises from respective breakdown or enhancement of the hydrogen-bonding network structure. Recent quasi-elastic neutron scattering measurements of the collective structural relaxation time, τ_C, in aqueous salt solutions were interpreted as confirming this explanation of the origin of ion effects on the dynamics of water. However, we find similar changes in τ_C in the same salt solutions based on MD simulations using a coarse-grained water model in which *no hydrogen-bonding exists*, challenging this conventional interpretation of mobility change resulting from the addition of salts to water. A thorough understanding of specific ion effects should be useful in diverse materials manufacturing and biomedical applications where these effects are prevalent, but poorly understood.

Introduction

Some combinations of anions and cations increase the self-diffusion coefficient (D) of water and others reduce it, while, correspondingly, the opposite trends arise for the shear viscosity (η) of the entire aqueous salt solution.[1–4] Ions are operationally termed *chaotropic* and *kosmotropic*, based on whether η is decreased or increased,[5] an effect historically interpreted as being due to structure-breaking and structure-making of the hydrogen-bonding network.[1,6,7] It is also implicit in these arguments, rationalizing specific ion effects, that an increase in solvent structural ordering and associated densification is responsible for this type of η enhancement[8] so that density-based free volume models have also been applied with some frequency to aqueous salt solutions.[1] Such arguments have been repeatedly made, despite the fact that increasing the density of water can in some instances increase water mobility.[9,10] In contrast, chaotropic ions are supposed to give rise to less ordering of the hydrogen-bonding network (corresponding to a reduction of density in a free volume structural framework[11]) to rationalize the lowering of η and the increase of D.[1,2,6] The differing behavior of chaotropic versus kosmotropic salts has provided the basis of many applications with stimuli responsive systems, controlled assembly, and a wide range of interfacial phenomena.[12–21] There is extensive and a rapidly growing literature discussing the specific ion effects on the dynamics and thermodynamics of water that we do not attempt to summarize in here. Many of the numerous applications and the theories proposed to rationalize this phenomenon have been thoroughly reviewed by Gregory *et al.*,[4] and we refer the interested reader to their work for this background information.

From the perspective of the presumed structure-making and breaking impact of salts on the hydrogen-bonding network, some researchers have equated the common observation of the increase in η upon the addition of some salts to an increase in the effective applied atmospheric pressure, since this was also anticipated to increase the density of water.[1,22,23] However, both neutron diffraction and X-ray measurements have suggested that this free volume based structural viewpoint of specific ion effects is inadequate.[23–25] In particular, little structural change (in terms of pair correlation functions) from the presence of ions seemed to occur beyond the first hydration shell: so that the effect of the ion on this type of structure appears to be highly local. Other spectroscopically-based measurement studies of aqueous salt solutions likewise concluded that a perturbation of the local "structure" of water, defined in terms of the rotational dynamics of the water molecules, was limited to the first solvation shell,[25,26] leading to debate of the ion structure-breaking and making paradigm for specific ion effects in aqueous salt solutions. The question of what extent ions influence the surrounding water, and how such changes impact the dynamical properties, evidently remains largely unresolved.[1,27–29] Nonetheless, it is clear from numerous previous

studies that changes in the properties of water with the addition of salts are conventionally interpreted as resulting from the impact on the literal structure of water's hydrogen-bonding network.[1,25]

In the present work, we agree that the influence of added salts on the hydrogen bond dynamics are symptomatic of specific ion effects related to changes in water mobility by salts, insofar that the addition of salt to water changes the macroscopic thermodynamics and transport properties of water in such a way that both the hydrogen bonding dynamics on sub-ps timescales and the effective interaction strength between the water molecules are altered. The effect of salts on the cohesive energy density of water can be modeled by coarse-grained classical molecular dynamics (CG-MD) simulations as well as the impact of these changes on the dynamics and thermodynamics of the fluid arising from these additives. This is the essence of our simulation strategy, which we discuss at greater length in the Conclusions section, after presenting our results.

One of the main purposes of the present work is to demonstrate that observed specific ion effect trends in water mobility, solution shear viscosity, and the structural relaxation time, do not require the explicit inclusion of hydrogen-bonding dynamics in our classical MD modeling. Of course, we do not intend to minimize the significance of hydrogen-bonding interactions in water,[30] as briefly just mentioned. Instead, we wish to systematically compute mobility changes in water with the addition of ions to highlight the importance of changes in the cohesive energy density of aqueous solutions as being the ultimate cause of chaotropic and kosmotropic effects. This interpretation does not contradict the prevailing idea that such changes are due to some sort of change in water's "structure". In fact, changes in water's "structure", have been conceptualized in terms of a change in the local cohesive energy density (CED) has been advocated previously,[31,32] although this interpretation of specific ion effects is not currently prevalent. It is evident that part of the controversy arising in this area relates to the ambiguity and adaptable meaning of the term "structure".[8]

Andreev *et al.*[33,34] recently observed that the change of D with respect to salt type, relative to pure water D_0, could be semi-quantitively estimated at room temperature from a coarse-grained (CG) model of aqueous monovalent salt solutions in which the water molecules were modeled by Lennard-Jones (LJ) particles. The success of this model is owed to representing the ion-solvent interaction strengths to be consistent with observed ion solvation energies. In this CG model of aqueous water solutions, the ion-solvent, solvent-solvent, and ion-ion bead interactions are described with a LJ potential well-depth parameter: $\epsilon_{i,w}$, $\epsilon_{w,w}$, and $\epsilon_{i,i}$, while ion-ion LJ interactions are superimposed on the Coulombic interaction potential between the ions. The different sizes of the ions and the water beads are taken to be equal for simplicity. The well-depths for the ions were set from scaling their respective Born radii to the reference KCl, known to have minimal impact on the transport properties of water, and thus may be considered as a

phantom ion in this restricted sense. In this way, the free energy of solvation (for which the inverse of the Born radii are a proxy) accounts for the various factors known to contribute to ion solvation, e.g., solute size and the degree of hydration[11]. Within this idealized model, ϵ_{iw} is the only variable that distinguishes between salt types. This minimal model of electrolyte solutions is an improvement over any theoretical treatment neglecting the solvent altogether. Indeed, this CG model was found to not only reproduce essential trends[33] in the change of D and η with the addition of salts spanning the full range from strongly chaotropic to kosmotropic, but remarkably, this model was also able to reproduce essential trends in the surface tension, density, and isothermal compressibility with the same series of salts.[34]

By contrast, no previous classical MD simulation of aqueous solutions had been able to explain even the *existence* of chaotropic ions.[35–37] Capturing this phenomenon requires models derived from first principles,[38,39] machine-learning[40] based forcefields, or forcefields involving scaled charges rationalized to capture polarization and charge transfer effects,[41,42] in addition to some polarizable models[42]. While first-principles studies have indicated that polarization plays a more prominent role than charge transfer,[43] either case will justify the use of scaled ion charges in aqueous solutions.[41,42] Although these methods capture kosmotropic/chaotropic trends they have not offered any clear physical interpretation of what allows these strategies to propagate from ion-solvent interaction to the transport properties of the system. The CG LJ model of salt solutions then offers a path forward for understanding the fundamental origin of both mobility and thermodynamic changes in aqueous solution properties upon adding salts to water. Since the free energy of solvation is the source of the parametrization of this model, the influence of ion size, electronegativity, charge transfer, and polarization are implicitly accounted for. Addressing the origin of these specific ion effects, however, requires that we consider collective diffusive and structural relaxation in aqueous salt solutions because properties of liquids generally involve such processes over a wide range of timescales.

We next turn our attention to examining an experimental study of collective diffusion and relaxation in aqueous solutions with added chaotropic and kosmotropic salts and compare those results to simulations based on the CG model just mentioned. A recent quasi-elastic neutron scattering (QENS) study[27] measured the structural relaxation time of water in aqueous solutions with both chaotropic and kosmotropic alkali metal ions and concluded that changes in the rate of water's collective relaxation should be attributed to the influence of the ions on the hydrogen-bonding network. The concept of "structure" here apparently refers in a generally way to the collective dynamics of water and its hydrogen-bonding network, but the exact nature of the "structure" that might be involved is unspecified, and thus open to interpretation. In this way, the sophisticated QENS measurements were claimed to be in accord with the traditional rationalization of specific ion effects as arising from a disruption in the structure of the water hydrogen-bonding network, as discussed above. Moreover, Liu *et al.*[27] found that the bulk solution hydrogen bond

lifetime showed no detectable dependence on salt type or salt concentration in their QENS measurements of the same system in which they showed concentration dependence of the collective structural relaxation time. Although, specific ion effects are known to occur for other aspects of the hydrogen bonding network that are on the fs timescale.[44–46] It was this neutron scattering by Liu *et al.* that prompted us to study whether the CG solution model of Andreev *et al*.[33,34] could reproduce the observed dependence of the collective structural relaxation time, τ_C, as a function of the salt type and concentration in accord with the dynamic neutron scattering measurements. This classical MD model does not involve hydrogen-bonding interactions, so the continued success of this model in capturing specific ion effects would be instructive on the essential aspects of such phenomena.

In the present work, we estimate the collective relaxation time, τ_C, i.e., structural relaxation time, for the same chaotropic and kosmotropic ions as those study via QENS measurements,[27] in a concentration range between 0.1 mol/L and 3 mol/L. We find semi-quantitative agreement between this CG aqueous solution model and the coherent neutron scattering measurements in the relatively low concentration range where the model is most suitable because of the current CG model's neglect of inter-ion dispersion interactions. Because the attribution of viscosity changes to the hydrogen-bonding network stemmed from an assumed constant infinite-frequency shear modulus, G_∞ in experiments,[27] we also test this assumption, finding similar variation of G_∞ to other solvent properties. After demonstrating that the observed changes in structural relaxation times do not by themselves implicate changes in hydrogen-bonding as their source, we show the linear relationship between the concentration-dependent change in η, D, τ_C, and G_∞, for different salt types and the difference between ion-solvent and solvent-solvent interaction energies. This linear relationship is then derived analytically in the supplementary information, and the result presented here. We then examined the physical nature of the ion hydration layer of kosmotropic and chaotropic ions, with this CG model, by drawing on analyses of the Debye-Waller parameter $\langle u^2 \rangle$, utilized in polymer glass-forming liquids to quantify mobility gradients around inorganic nanoparticles,[47] and more recently in studies of solvated systems[48–50]. Following previous researchers, we define $\langle u^2 \rangle$ as the mean-squared displacement (MSD) of the particles on a characteristic caging timescale, t_C, a timescale on the order of a ps in molecular fluids. The value of $\langle u^2 \rangle$ has been directly related to the incoherent structural relaxation time in simulation studies,[51,52] also demonstrated in this work. However, $\langle u^2 \rangle$ can also be analyzed as a per particle quantity to analyze dynamic heterogeneity in solvated systems,[48–50] which shows significant differences between chaotropic and kosmotropic ion hydration. Given that the dynamic hydration layers are extended around the ions, there must come a point with increasing concentration where the hydration layers overlap, we find that the 1st hydration layers in this CG model percolate at relatively low

concentration so the extended influence of the interaction energy between salt and solvent to propagate at the concentrations in question.

Methods

This work models solutions with varying concentrations of alkali metal salts with a coarse-grained molecular dynamics (CG-MD) approach. Three independent boxes allowed for statistical analysis, and were built at each salt concentration with the MosDef[‡] suite (i.e., mbuild[‡,53] and foyer[‡,54]). Each simulation box then contains 10 054 CG beads where the fraction that represents salt is dependent on the target concentration of (0.1, 0.5, 1, 2, 3) mol/L. The CG beads interact through a Lennard-Jones (LJ) potential where all values are equal to unity in LJ units unless otherwise specified. This study focuses on a series of cations with Cl^- as a counter-ion with an interaction energy of one, $\epsilon_{Cl,w} = 1$. The cations range in their cross interaction energy parameters according to their scaled Born radii relative to K^+, as explained in previous work.[33] The condition in which $\epsilon_{i,w} = 1$ corresponds to a *phantom* ion reference case in which the ion is assumed to have no effect on the mobility of water, which is clearly just an approximation that holds over a limited range of *T*. This methodology of estimating the solvent-ion interactions without fit parameters, also assumes that the anions and cations contribute independently to the alteration in the water mobility, a property shown to hold to a good approximation for many simple ions at low salt concentrations.[55,56] Ion association at high salt concentration can be expected to invalidate this assumption where ion specific effects of anion-cation interactions should be incorporated into the modeling through osmotic virial coefficient data of electrolyte solutions or other observations sensitive to ion association. The modeling that we consider is limited to a temperature range well above the melting temperature where the complex dynamics of supercooled water are not prevalent[57] and strictly speaking should be limited to a regime where the concentration dependence of water's transport properties are not heavily driven by ion-ion interactions. This methodology for estimating the ion-solvent dispersion interaction strength for Na^+ (kosmotropic), K^+, and Cs^+ (chaotropic) results in values of 1.25, 1, and 0.85, respectively, in LJ units with a potential cutoff of $r_C = 3\ \sigma$. To represent the charge interaction between the ions, a dielectric constant of 0.771 was used to scale the charges to produce a Bjerrum length of 1.73 σ at $T^* = 0.75$, where σ is expected to be 0.4 nm.[33,34] The characteristic timescale for this LJ system, τ, is on the order of a ps, consistent with the Debye-Waller parameter for water models used in atomistic simulations.[50]

MD simulations were carried out with the Large-scale Atomic/Molecular Massively Parallel Simulator (LAMMPS)[‡,58] using periodic boundary conditions. Long-range electrostatics were treated using a particle-particle particle-mesh solver[59] with a relative error of 0.0001. Three independent configurations for each salt type and concentration were equilibrated for 3 000 τ with a timestep of 0.005 τ and constant

temperature and atmospheric pressure (*NPT*) at $T^* = 0.75$ and $P^* = 0.01$. The last 500 τ was used to calculate the equilibrium box size for subsequent simulations in the canonical ensemble (i.e., constant volume and temperature, *NVT*), 23.37 σ. After 10 000 τ of equilibration with a decreased timestep of 0.001 τ, a production run of approximately 23 000 τ was used for the analysis in our work, as dynamic properties are most reliably represented in the *NVT* and microcanonical (i.e., constant volume and energy, *NVE*) ensembles.[60,61] The Nose-Hoover thermostat and barostat were utilized with respective dampening factors of 1.0 and 10.0), where applicable. The analysis results of this work were produced in LAMMPS[‡,58] with the aid of MDAnalysis[‡,62,63]. The viscosity was computed from the system pressure tensor written every 0.01 τ using the recommended Green-Kubo relation, details described elsewhere.[60]

Results and Discussion

A recent quasi-elastic neutron scattering (QENS) study of salt solutions[27] has provided insight into the structural relaxation of water depending on salt type and concentration. Until this work, most neutron diffraction studies of salt solutions focus on isotopic substitution to ascertain the pair distribution function of ions and their solvation layers.[22,64–66] Such a strategy provides information on the number of water molecules in the first hydration layer and their average orientation, where structural information beyond that layer is undiscernible except in the case of the second hydration layer of bivalent ions such as Ni^{2+}.[64] Previously, incoherent QENS measurements have been used to study *D* for ionic solutions,[2] confirming known changes relative to pure water from nuclear magnetic resonance (NMR) measurements. In temperature-dependent studies of water, two relaxation times have been identified from incoherent QENS measurements, thought to be associated with hydrogen-bond fluctuations and structural relaxation in addition to a vibrational component.[67,68] It is only recently that Luo *et al.*[27] evaluated the structural relaxation of ionic solutions with coherent QENS, taking collective relaxation under consideration. That work also determined the relaxation times of hydrogen-bond fluctuations and structural relaxation, concluding that the addition of various concentrations of NaCl, KCl, and CsCl do not affect the former. The finding that relaxation times characteristic of hydrogen-bond lifetimes are invariant with salt type and concentration seems to be inconsistent with the conclusion that kosmotropic or chaotropic ions cause a constructive or destructive effect on the hydrogen-bonding network. However, the longer structural relaxation times varied with ion concentration similarly to the viscosity changes, as one might expect. The experimental conclusions of Luo *et al.* are perplexing from the existing evidence that chaotropic and kosmotropic ions influence the transport properties of water through their effect on the hydrogen-bonding network, yet they provide credence to the results of the LJ model of Andreev and coworkers,[33,34] capturing the essential physics of alkali metal ion solutions.

In order to compare the collective structural relaxation time of water reported by Luo *et al.*[27] to the LJ model of Andreev *et al.*[33,34], we computed the collective intermediate scattering function, $F_C(t)$. The isotropic approximation of $F_C(t)$ was applied,[69–71] which is expected to result in quick convergence and the flexibility to be computed at any q-value.

$$F_C(t') = \frac{1}{M}\sum_{m=1}^{M}\frac{1}{N}\sum_{i=1}^{N}\sum_{j=1}^{N}\frac{\sin\left(q\, r_{ij}(t')\right)}{q\, r_{ij}(t')}\delta_{ij}(t,L) + C(L) \quad (1)$$

The intermediate scattering function calculation (Equation 1) is limited to the sphere around each particle with a diameter equal to the simulation box of length, L, by the delta function, $\delta_{ij}(t,L)$, with corrections, $C(L)$.[69–71] The distance between a bead at an initial time and all other beads after some time lag, *t'*, is summed, and then averaged over particles, N, and simulation frames, M, result in the final $F_C(t)$. These intermediate scattering functions were calculated at a q-value of 6.68 σ^{-1}, or the peak of the static structure factor, approximately at the particle length scale. Because $F_C(t)$ was found to be nonexponential (as shown in other atomistic simulation studies[72]), the relaxation times were taken at the point that the normalized function, $F_C(t) / F_C(0) = 0.2$.[73,74] This relaxation time of the intermediate scattering function at the q-value corresponding to the peak in the static structure factor is commonly referred to at the structural relaxation time, providing a metric of fluid structure.

We observe that the success of this CG model of aqueous ion solutions introduced by Andreev *et al.*[33,34] continues as we compare the structural relaxation time taken from the coherent scattering function (i.e., collective intermediate scattering function), $F_C(t)$ to QENS measurements. It is observed that with increasing concentration, the spread between long time relaxation of the different salt solutions becomes more apparent. A comparison of this CG model to relaxation times taken from QENS measurements[27] shows qualitative agreement (Figure 1b). Notice that the simulation values (Figure 1b, left axis) and the QENS data (Figure 1b, right axis) are plotted on different scales, with a difference of a factor of two. Such agreement appears to breakdown at concentrations of 2 mol/L and 3 mol/L, illustrating the known issue with this model at high salt concentrations where ion-ion interaction parameters have not been tuned.[33] The continued agreement between this LJ model encourages confidence in the model's ability to provide insight into the ion concentration dependence of solvent transport properties.

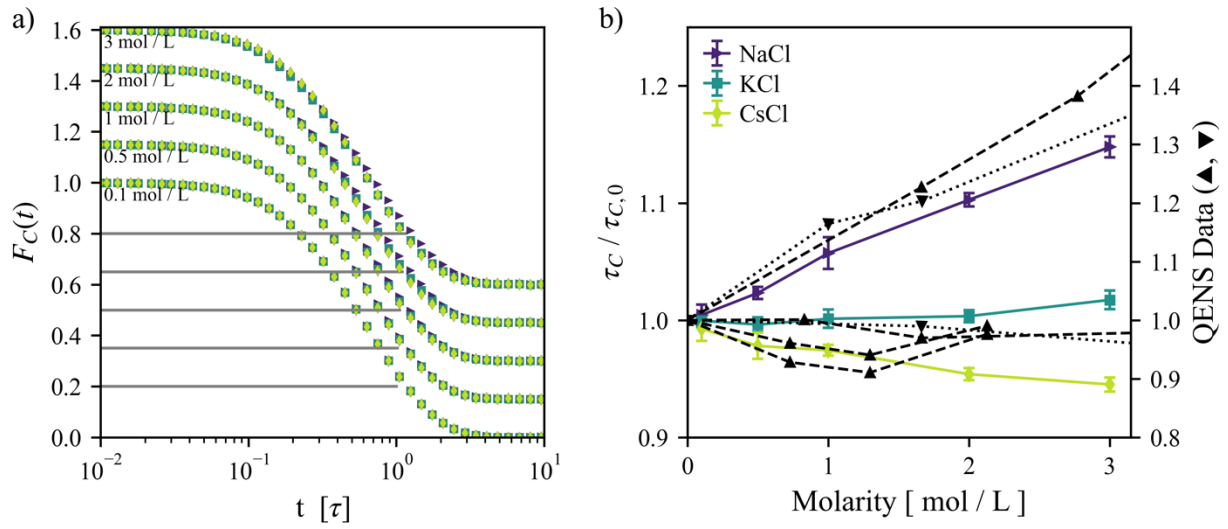

Figure 1: (a) Collective intermediate scattering function for studied salt combinations where the horizontal lines (gray) indicate values of τ_C at which $F_C(t) = 0.2$[73,74]. Trends at different concentrations are shifted up by 0.15 for clarity. (b) The changes in τ_C are plotted alongside QENS data[27], where the two axes illustrate that our simulated relaxation times relevant to pure solvent approximately scaled to half the relative relaxation time from experiments. QENS measurements shown in black represent measurements from two neutron sources described elsewhere.[27] Uncertainty intervals represent the standard deviation between replicate simulation runs.

To further discern the source of the salt concentration dependence on the viscosity and structural relaxation, Luo *et al.*[27] probed the ratio between the two properties. The meaningfulness of this ratio, η/τ_C, stems from a common adaptation of the Stokes-Einstein relationship[75–77] where viscosity is replaced with the structural relaxation time from coherent[76] or incoherent[75,77] neutron scattering measurements, thus, $\tau_C \propto \eta$. Assuming the structural relaxation time also scales with the stress relaxation time,[78,79] the ratio η/τ_C was expected to provide insight into the ion concentration dependence of G_∞. Such an assertion stems from the Maxwell relaxation, $\eta = \tau_M G_\infty$, where η is assumed to be described by a single relaxation process characterized by the Maxwell relaxation time, τ_M.[80] Luo *et al.* examined the ion concentration dependence of G_∞ by plotting the ratio of viscosity, η/η_0, and relaxation time, $\tau_C/\tau_{C,0}$, where each property was scaled by their value for pure solvent. The ratio of scaled viscosity to scaled relaxation time varied from approximately 0.9 to 1.1 in a scattered manner, suggesting that G_∞ was indeed constant. As shown in Figure S1, our calculations show a similar range of variation but with the same ion concentration dependence observed for the structural relaxation times. In addition to this indirect evaluation of G_∞, our simulation study allows for a direct calculation of G_∞ through the breakdown of the Green-Kubo relationship of the stress autocorrelation function (ACF),[81]

$$\tau_M\, G_\infty \approx \eta = \frac{V}{k_B T}\int_0^\infty \langle \sigma^{xy}(0)\sigma^{xy}(t)\rangle dt, \tag{2}$$

$$G_\infty = \frac{V}{k_B T}\langle \sigma^{xy}(0)\sigma^{xy}(0)\rangle, \tag{3}$$

$$\tau_M = \int_0^\infty \frac{\langle \sigma^{xy}(0)\sigma^{xy}(t)\rangle}{\langle \sigma^{xy}(0)\sigma^{xy}(0)\rangle}\, dt, \tag{4}$$

where σ^{xy} represents the off-diagonal elements of the system stress tensor. Note that there is discussion in the literature whether the *affine* modulus, G_∞ (calculated from Equation 3) is comparable to the high-frequency plateau G_∞ taken from experimental studies,[81] but for the purposes of this work, we use the definition of the infinite-frequency modulus in Equation 3. An analytical estimate of G_∞ can also be computed for a LJ model based on an expression derived by Zwanzig and Mountain,[82]

$$G_{\infty,\mathrm{ZM}} = 3P + \frac{26}{5}\rho k_B T - \frac{24}{5}\rho\langle E\rangle, \tag{5}$$

where P, T, ρ, and $\langle E\rangle$ represent the pressure, temperature, number density, and average total energy, respectively. This expression was derived for a homogeneous LJ liquid, and so here, Equation 5 provides a naïve estimate via $G_{\infty,\mathrm{ZM}}$ that neglects the multicomponent nature of the salt solutions and the presence of ion-ion Coulombic interactions, an approximation in the spirit of the origination of the CG model of aqueous salt solutions. Notice that the summation of the second and third terms of Equation 5 are approximately proportional to the CED, which is defined as the inter-molecular energy of the system.[83,84] Since there is no intra-molecular energy in our system, the CED from simulations is simply the potential energy times the number density, i.e., number density times the difference between the total energy and the kinetic energy, where the prefactors in Equation 5 with the conversion of temperature to kinetic energy are relatively close in value. A comparison between $G_{\infty,ZM}$ and the CED in Figure S2 and between G_∞ from Equation 3 and $G_{\infty,ZM}$ from Equation 5 is shown in Figure 2a.

Notice that the variation in the stress ACF and G_∞ (Figure 2a) with respect to salt type and concentration. While the stress ACF for only the lowest and highest ion concentrations is shown for clarity, the change in G_∞ (Figure 2a inset) is shown to reliably vary to a greater extent than Figure S1, which should be equivalent if η/τ_C were a reliable proxy for G_∞. G_∞ is also often presumed to be constant with temperature, although other simulations of LJ and atomistic systems have shown that this is not the case.[82,85,86] Considering that G_∞ is proportional to the mean-squared stress of the atoms, it is no wonder that by increasing and decreasing the interaction energy respectively between solvent and kosmotropic and chaotropic salts that we find this variation (Figure 2a inset). Indeed, our crude estimate of $G_{\infty,ZM}$ from Equation 5 (Figure 2a inset, dashed line), without taking the ternary system or Coulombic interactions correctly into account, also exhibits kosmotropic and chaotropic trends. The combination of the second and

third terms of Equation 5 is nearly equal to the CED of the system (Figure S2) and represents nearly all this analytical estimate for G_∞. Indeed, Figure S2a shows that $G_{\infty,ZM}$ closely follows the relative changes in the cohesive energy density (defined as the intermolecular potential energy per unit volume[87–89]) of our simulations. Future work might involve properly representing the specific ion effects neglected in this estimate.

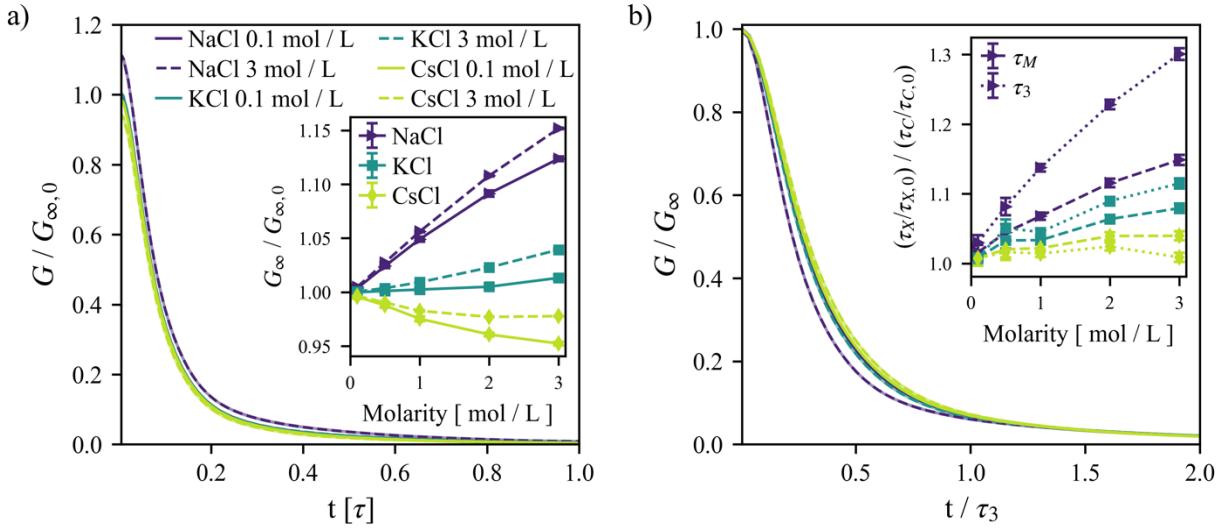

Figures 2: (a) Stress autocorrelation function for salt solutions at 0.1 mol/L and 3 mol/L scaled by the infinite-frequency shear modulus, G_∞, for pure solvent. Inset: G_∞ for each salt solution with respect to salt concentration from simulations (solid line) and from a crude analytical estimate in Equation 5, $G_{\infty,ZM}$[82] (dashed line). (b) Stress autocorrelation function for salt solutions at 0.1 mol/L and 3 mol/L scaled by their respective values for G_∞, and an abscissa scaled by their respective longest relaxation times, τ_3. This scaling of the abscissae is further discussed in Section S2 of the supplementary material. Inset: Stress relaxation times, τ_X, scaled by the structural relaxation time for each salt solution with respect to salt concentration, where X is one of the timescales defined in the legend. Uncertainty intervals represent the standard deviation between replicate simulation runs.

Returning to our assessment of system relaxation, we then calculate the ratio between the stress relaxation times and τ_C (inset of Figure 2b) where the stress relaxation time is expressed as either τ_M or the longest of three relaxation times (τ_3) identified in the stress ACF (Equation S1). The Maxwell model definition of τ_M from Equation 4 varies similarly to τ_C, even as the stress ACF involves three distinct relaxation times in governing relaxation in these complex solutions. Similar results have been reported elsewhere supporting the use of the Maxwell relaxation model as a simplified model of general utility.[90] The two faster relaxation modes were found to be consistent among all system conditions such that only G_∞ and τ_3 varied with salt type and concentration. Nonetheless, just as the structural relaxation time is

taken to be the long time relaxation of $F_C(t)$, so too should the characteristic stress relaxation time.[90] Although, we find that τ_3 varies more with system conditions than τ_C. Figure 2b shows how τ_3 may be used to illustrate time-salt superposition, a concept important to understanding the rheology of polyelectrolyte complex or coacervate solutions,[91–93] and we expand on this topic in Section S2 of the Supplementary Material.

After establishing that G_∞ varies with salt type and concentration due to changes in the CED through Equation 5, it is then enlightening to compare these effects to other properties through *B*-coefficients. This coefficient stems from the Jones-Dole equation[94] for quantifying chaotropic and kosmotropic trends in viscosity variation for aqueous solutions,

$$\eta/\eta_0 = 1 + A\sqrt{C} + BC, \tag{6}$$

where η_0 is the viscosity of pure solvent and C is the salt concentration in mol/L. The A-coefficient term in Equation 6, derived from Debye-Hückel theory,[95] is much smaller than the B-coefficient, which describes the leading linear salt concentration dependence, so A can reasonably be (and often is) neglected. Chaotropic salts are then defined by a negative B-coefficient and kosmotropic salts by a positive value. Because the linear concentration dependence between 0.1 mol/L and 1 mol/L is found to be consistently present for η, G_∞, τ_C, and D, we fit a B-coefficient to each property for easy comparison in Figure 3.

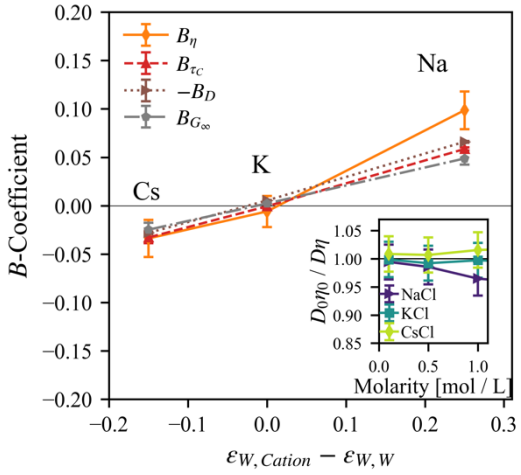

Figure 3: *B*-coefficients describing the concentration dependence of the viscosity, structural relaxation time, τ_C, and self-diffusion coefficient of solvent where the changes are plotted against the difference in the ion-solvent and solvent-solvent interaction energies. Inset: Stokes Einstein relation scaled by that of pure solvent. Uncertainty intervals represent the standard deviation between replicate simulation runs.

The approximate applicability of the Stokes-Einstein relation[96,97] between D and η of aqueous solutions near room temperature implies a corresponding relationship between the leading concentration virial coefficients of these basic transport properties. In particular, the prediction that the B-coefficients of each of these properties should be simply equal in magnitude, to a good approximation. The inset of Figure 3 shows that this relation holds particularly well at low salt concentrations. Although the B-coefficient has historically been discussed in relation to the linear changes in the shear viscosity leading order with respect to salt concentration (with some exceptions), we extend this definition to describe the virial coefficients describing the leading order concentration dependence of the properties τ_C, G_∞, and D. We also discuss how these generalized B-coefficients are interrelated. In line with this type of relation, recent NMR relaxation time measurements have indicated a B-coefficient that closely paralleled the viscosity B-coefficient in its variation with specific salts.[56]

An understanding of changes in relaxation processes and transport properties with the addition of salt ultimately derives from a consideration of how the B-coefficient depends on the molecular parameters of this CG water model. The answer to this question turns out to be quite simple as Figure 3 demonstrates a linear dependence between the B-coefficients and the difference between ion-solvent and solvent-solvent interactions energies,

$$B \approx A_o\,(\epsilon_{i,w} - \epsilon_{w,w}) + B_o, \tag{7}$$

where A_o and B_o are 0.25 ± 0.02 and 0.00 ± 0.00, respectively, after fitting the plotted trends. The intercept happens to be zero so that the B-coefficient for the reference salt system, KCl, which is the reference anion and cation used to scale the ion-solvent interactions of this forcefield,[33,34] due to the minimal known effect on water's transport properties for this salt pair. This result aligns with our assertion that specific ion effects arise from the interaction energy between the ion and solvent. Equation 7 applies to all the properties considered in our discussion above. Thus, the B-coefficient varies linearly with the difference between the well depths describing the ion-solvent and solvent-solvent interactions. We have provided a derivation of this expression in the supplementary material leading to the expression:

$$B_{\tau_C} \approx (\epsilon_{Cation-S} - \epsilon_{S-S})\frac{K}{\rho^* T^*} \tag{8}$$

where ρ^* and T^* are the number density and temperature in LJ units respectively. The precise value of proportionality constant K between the interaction energy of the LJ beads and the resulting activation energy of the solution, depends somewhat on the method of estimating the activation energy.[98,99]

Within this CG model, the changes in D, η, τ_C, and G_∞ all arise from a change in the CED of the fluid, a phenomenon naturally associated with the change in $\epsilon_{iS} - \epsilon_{SS}$. Likewise, studies of homogeneous LJ fluids have demonstrated that changes in the interaction energy well-depth (ϵ), in a leading order of

approximation, correspond to a linear variation in the height of the radial distribution function's (RDF) primary peak at a fixed temperature.[100] We might then expect the difference in the primary peak heights of the cation – solvent RDF and the solvent-solvent RDF to directly reflect the change in ion-solvent interaction energy strength, $\epsilon_{i,w}$- $\epsilon_{w,w}$ in the same single LJ fluid approximation as utilized above. Consistent with this expectation, Figure S3 shows that the changes in height of the primary peak of the RDF in our simulated ionic solutions exhibit a near linear relationship with the *B*-coefficients at low salt concentrations. Evidently, changes in the height of the RDF thus provide valuable information about the interaction strength of ions with the solvent. In consistency with the findings just mentioned, Corridoni *et al*.[8] have emphasized that the influence of ions on the structure of water is almost exclusively limited to first hydration layer, corresponding to a scale on the order of the peak position of the RDF, and that ions have little discernable structural influence on local density-based measures of water "structure".

The collective relaxation time, τ_C, of particular interest in the present work has been previously shown to be highly correlated with G_∞. In particular, the phenomenological *shoving model* relates these quantities.[101,102] Specifically, this model of τ_C assumes that the activation energy ΔE_A for a molecule to escape from its local cage should be approximately equal to the shear elastic energy cost for this displacement leading to the estimate,

$$\tau_C = \tau_{C,0} \exp\left(\frac{\Delta E_A}{k_B T}\right) \approx \tau_{C,0} \exp\left(\frac{V_C G_\infty}{k_B T}\right), \tag{9}$$

where V_c is an unspecified volume on the order of the molecular volume that is temperature independent. While this model is clearly not exact, it aids understanding of essential trends in τ_C. We can see that a combination of Equation 5 and Equation 9 would indicate the activation energy increases with the CED. The same reasoning underlies the assumption by Eyring and coworkers[103] that ΔE_A should be proportional to the heat of vaporization, another property closely related to the CED. In order to take this argument further, we may exploit another relationship that has become appreciated more recently relating G_∞, and thus τ_C, to another high-frequency dynamics property, the particle MSD on a caging timescale, or the Debye-Waller parameter, $\langle u^2 \rangle$ of the solvent.[52,101] In particular, Leporini and coworkers[104] have found that G_∞ in Maxwell's relation can be approximated as, being linear in $k_B T / \langle u^2 \rangle$, and thus the relaxation time can be approximated as,

$$\tau_C \propto \tau_{C,0} \exp\left(u_0^2 \Big/ \langle u^2 \rangle\right) \tag{10}$$

where u_0 is an empirical constant. A similar mathematical relation,[48,105–108] between τ_C and $\langle u^2 \rangle$ has been derived from independent arguments emphasizing dynamic free volume $v_f \sim \langle u^2 \rangle^{3/2}$ in which τ_C is predicted to scale as $\exp[(u^2_o / \langle u^2 \rangle)^{3/2}]$ or with a variable exponent α, i.e., $\exp[(u^2_o / \langle u^2 \rangle)^{\alpha/2}]$. The inset in Figure 4a

indicates that a $1/\langle u^2 \rangle$ scaling (i.e., $\alpha = 2$) holds for the salt concentration dependence of both chaotropic and kosmotropic ions in this CG water model. The generality of this scaling for other models of water remains to be seen. Nonetheless, use of this formalism illustrates the utility of the Debye-Waller parameter, where its value has been considered a measure of local mobility[47–52,109,110] and its inverse a measure of local material stiffness[47,104,111].

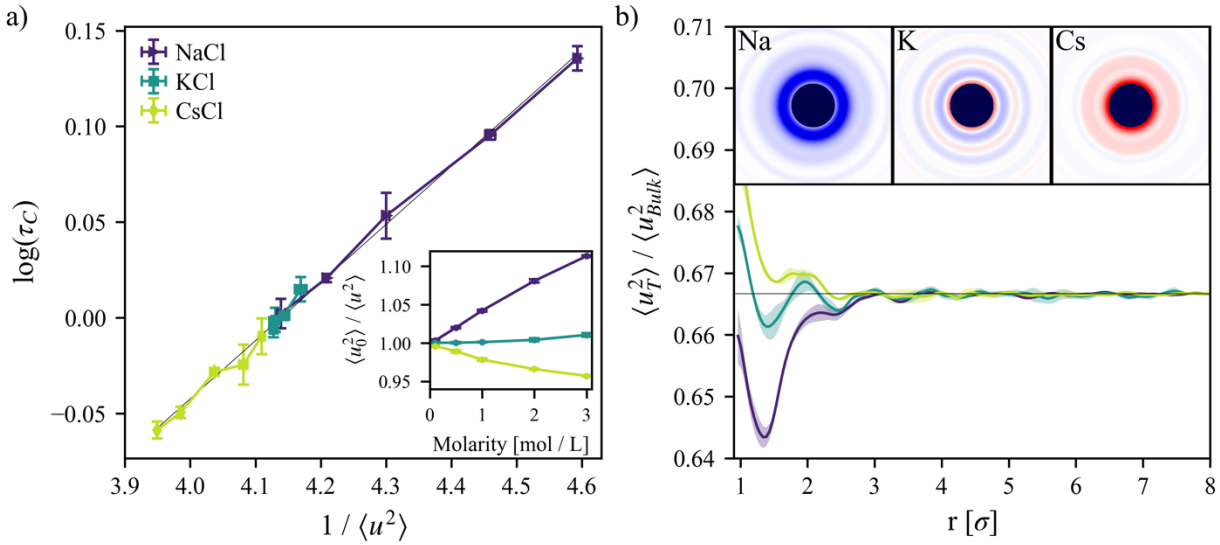

Figure 4: (a) Relationship between τ_C and the Debye-Waller parameter of the solvent, $\langle u^2 \rangle$. Inset: Variation in $1/\langle u^2 \rangle$ with respect to molarity. (b) Radial tangential components of $\langle u^2 \rangle$ around Na^+, K^+, and Cs^+ in dilute solution (C < 1 mmol/L) scaled by the total bulk value. Inset: Heat maps of smoothed $\langle u_T^2 \rangle / \langle u_{Bulk}^2 \rangle$ at radial distances from ions, where the tangential components make up two thirds of the total. Uncertainty intervals represent the standard deviation between replicate simulation runs.

Unlike the other macroscopic properties evaluated in this work, $\langle u^2 \rangle$ can be examined on a molecular or atomic basis, allowing for the definition of a local measure of mobility.[50] $\langle u^2 \rangle$ is taken to be the mean-squared displacement on the caging timescale 0.8 τ (see Supplemental Information for its precise estimation). In Figure 4b, we show the variation in the tangential component of the $\langle u^2 \rangle$ radially from an ion in dilute solution (C < 1 mmol/L). The magnitude of the radial component is smaller, making less of a contribution to the overall average $\langle u^2 \rangle$ (Figure S5). Figure S5 shows the radial dependence of the total $\langle u^2 \rangle$, as well as the normal component for comparison. In each case it is evident that $\langle u^2 \rangle$ changes radially from the ion, where fluctuations indicate solvation layers which become more obscure with increasing distance from the ion as averaging over a larger area becomes diffuse. Knowing that this is the mean-squared displacement on the caging timescale, it should be no surprise that it varies with the expected potential energy wells where the average displacement is smallest in the minimum and increases with

movement out of the well. A discussion on the implications of this work with the shoving model has been provided in the supplementary material. In all cases, Figure S5 shows that the tangential component of $\langle u^2 \rangle$ has the least variation for a given ion, suggesting fewer barriers of translational motion shown in Figure 5b, thus this component will be the focus of our discussion.

Considering the difference in interaction energy between the cations, it is no surprise that the mobility of solvent close to Na^+ is suppressed in the first hydration layer, however, the tangential component around Cs^+ is intriguing. It appears that the tangential mobility adjacent to chaotropic ions, in this case Cs^+, increases to the point where there is accelerated mobility up to 2.5 σ from the ion. Accelerated mobility around chaotropic ions was previously predicted by Collins and Washabaugh[5] and consistent with residence times of simulated solvation shells around chaotropic ions[112]. On the other hand, the lowered tangential mobility around Na^+ extends to 3 σ, the interaction cutoff used in our simulations. These results seem to align with other computational measures of the "softness" of the hydration layer around ions.[113] With increasing concentration, the radial effects of the ions observed here are expected to interfere with each other.

Applying the analysis used to generate Figure 4b becomes convoluted at higher ion concentrations as the distance between ions decreases, thus averaging $\langle u^2 \rangle$ per hydration layer provides the most accessible dimension of analysis, as done elsewhere.[50] The first hydration shell is defined by the first minimum in the radial distribution function, RDF, taken as 1.56 σ. Subsequent hydration layers are then defined by the subsequent minima, found to be approximately 1 σ apart. The hydration layer to which a solvent bead belongs is then defined by its closest distance to any ion. Figure 5 shows the change in the scaled Debye-Waller parameter for each salt combination. In the case of NaCl and KCl at 0.1 mol/L the first hydration layer is less mobile and then converges to a bulk mobility value with increasing distance from an ion, taking a value consistent with the expectation of a bulk value of unity. As the concentration of NaCl is increased the mobility of the first hydration layer continues to decrease, likely as the proportion of solvent in the first hydration layer increases (Figure S6) and is less disturbed by the shrinking proportion of solvent that is not in contact with the ions, or "free" solvent.[114] It has been plausibly suggested that the presence of hydration shells creates larger obstacles for the bulk solvent to diffuse around.[115] This would explain the decreasing mobility around Na^+ where a boundary layer with hindered mobility has an impact on bulk solvent that is decreasingly able to obtain space between itself and an ion, as well as the percolation of hydration layers.[28,116] Such a conclusion is supported by Figure 6 and represented in Figure S6.

Although it is easy to qualitatively anticipate how the percolation of the hydration shells around the kosmotropic ions might give rise to a large effect on ion and solvent mobility for the reasons just indicated, the effect of chaotropic ion, Cs^+, on the solution dynamics is more subtle (this percolation is

illustrated below). In the case of kosmotropic ions, the strong interaction of the ion with the solvent naturally localized the short time solvent dynamics (i.e., mobility) around this type of ion. Since the change of the energy density arising from an additive with a different cohesive interaction strength naturally propagates appreciably into the solvent,[117] the region over which the solvent mobility is modified, naturally forms a mesoscopic volume. Such a non-local effect on mobility of the surrounding liquid from additives is not at all limited to ions and water and has recently been studied in polymer nanocomposites.[47,118,119] The solvent dynamics around the chaotropic, Cs^+ ions are accelerated; apparently deriving from the reduction in the local interaction strength, $\epsilon_{Cs,W}$. However, the magnitude of this acceleration in the solvent dynamics is relatively weak so that the perturbation in the dynamics appears to occur more uniformly throughout the aqueous solution for this chaotropic ion. We note that ions having a more complex structure can be *superchaotropic*[15,120] and this phenomenon has been observed in certain charged proteins of significant biological interest[109,121] For such charged species, we may anticipate percolation of the hydration layers to give rise to highly accelerated mobility in extended solvent domains and thus to non-local changes in solvent mobility and large changes in the solution viscosity.

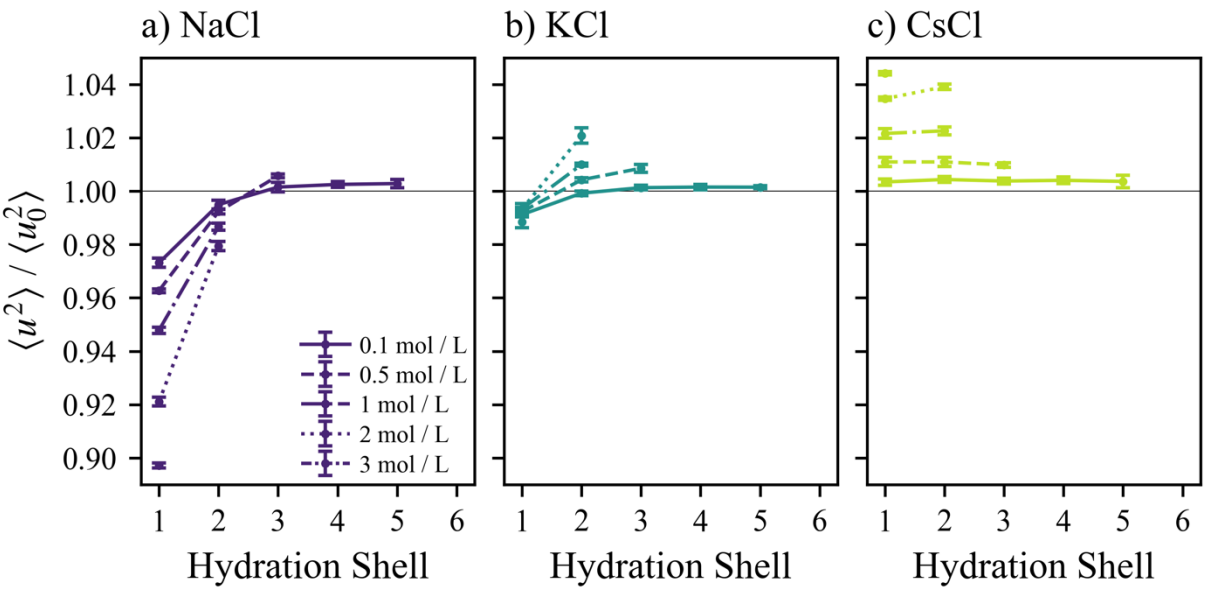

Figure 5: Changes in the Debye-Waller parameter of the solvent, $\langle u^2 \rangle$ reduced by $\langle u^2_0 \rangle$ for pure bulk solvent with respect to hydration shell number where each column represents the cation combinations: (a) NaCl, (b) KCl, and (c) CsCl, respectively. Uncertainty intervals represent the standard deviation between replicate simulation runs.

One of the interesting features apparent in Figure 5 is that while the ion type effects the mobility ($\langle u^2 \rangle$) in the hydration layer around the different types of ions, it is influenced in a highly ion specific way.

the spatial scale over which the mobility is altered is *remarkably insensitive* to ion type and ion concentration at these moderate salt concentrations, when comparing NaCl and KCl. This raises the question of what physical factors control the width of the interfacial zone around the ions where the solvent mobility is modified. Interestingly, this same insensitivity of the width of the interfacial zone to the interaction strength between reference and surrounding media has been observed upon adding nanoparticles to polymer matrices where a scale of perturbed mobility on the order of a nm has been observed in numerous simulations and measurements.[47,118,119] These nanocomposite studies also revealed that the mobility in the interfacial region can be either be increased or decreased relative to bulk values, depending on the relative strength of the polymer-nanoparticle to polymer-polymer interaction parameter strength so the interfacial zones in these problems seem to exhibit remarkable similarities in their phenomenology. Widom and coworkers[117] have argued that the scale of the interfacial region around additives to water are mainly set by the properties of the water molecules, in accord with our findings. The physical origin of the relative insensitivity of the interfacial zone width to the intermolecular interaction strength is thus evident. Future studies should explore exactly what molecular parameters of the suspending fluid control this characteristic scale. We next focus on quantifying percolation in the relatively simple limit of the phantom ion pair, K^+ and Cl^- to provide some qualitative insights into previous observations about the salt concentration dependence of τ_C.

The idealized limit of phantom anion and cations illustrated in Figure 6 provides a simple reference system with which to discuss purely geometric aspects of the percolation of the hydration layers around ions since the hydration layers of both ion types are indistinguishable. Luo *et al.*[27] suggested that deviations from the linear change of τ_C with respect to salt concentration at 3 mol/L for all ion species (Figure 1b) was the result of overlapping hydration layers. However, Figure S6a shows that nearly all solvent molecules in our simulations at this concentration are in direct contact with KCl ions so that the first hydration layers likely percolate at an even lower concentration. It is visually apparent that our lowest concentration, 0.1 mol/L KCl (Figure 6), is close to percolation of the ion static hydration layers (1^{st} hydration layer < 1.56 σ from an ion), while percolation is certainly achieved at a concentration of 1 mol/L. Indeed, Figure S6b shows that concentrations of all studied ions at 0.5 mol/L or greater, have completely percolated 1^{st} hydration layers. The overlap of the 1^{st} hydration layers at 1 mol/L KCl is visualized in Figure 6 to give some further insight. We also see from Figure S6b that the remaining two salt species exhibit a percolative transition at similar concentration, validating the use of the phantom ion model for the estimation of the percolation threshold as a reasonable approximation. The occurrence of percolation in these hydration layers should change the cohesive energy density of the solution so that the effect of the ions should no longer contribute additively to the solution properties. We may expect a strong non-linearity to arise in

superchaotropic ions at elevated salt concentrations or in water soluble macromolecules; these topics requiring future study.

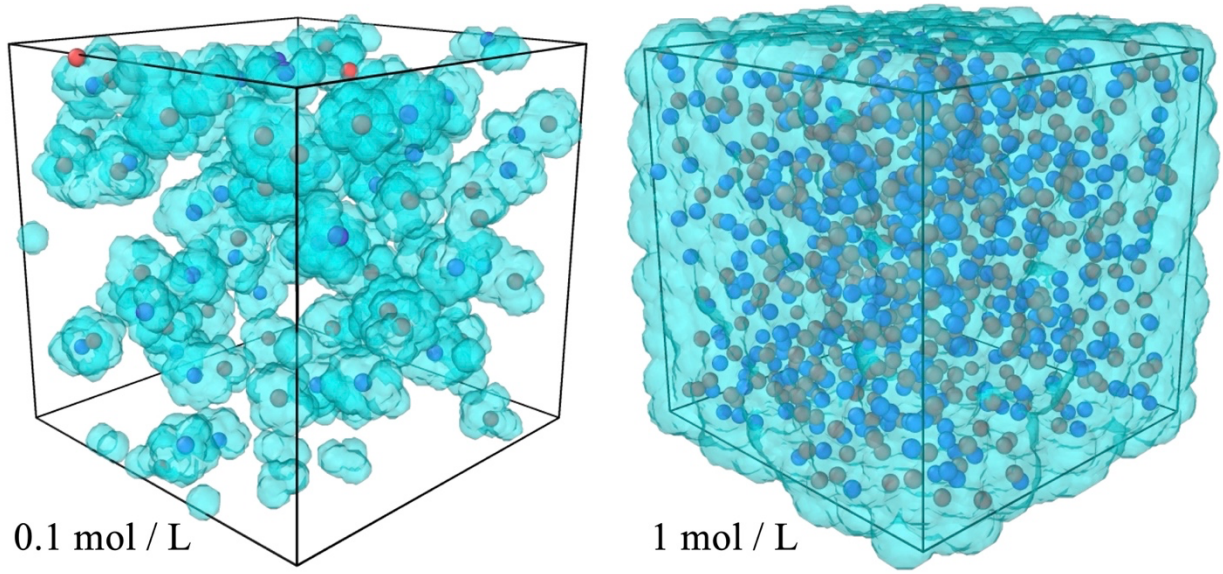

Figure 6: First hydration shell, i.e., static hydration layer, for solutions at 0.1 mol/L and 1 mol/L KCl. Blue and red spheres respectively represent the phantom ions, K^+ and Cl^-, which hydrate similarly to solvent molecules in pure solvent. All solvent molecules beyond the first hydration layer are not rendered for clarity.

It is admitted that the interaction energy parameters of this CG model of aqueous salt solutions are fixed by the solvation energy of the ions so the model involves *no free parameters*. Of course, the model involves several significant approximations such as the neglect of salt-specific potential interactions between the anions and cations that are no doubt important for ion association at elevated salt concentration, an approximation that limits the concentration range in which the model can be reasonably applied. Future extensions of the model to account for these inter-ion interactions could be made, in principle, based on osmotic pressure and activity measurements of salt solutions from which osmotic virial coefficients can be extracted.[122,123] Such an extension of the present CG aqueous salt solution model is left for future work.

Conclusions

We find semi-quantitative agreement between QENS measurements[27] and the LJ model for salt concentrations between 1 mol/L and 3 mol/L. Given the simple nature of the LJ model without hydrogen-bonding interactions. Clearly, the observed mobility changes in aqueous solutions upon adding salt to solvent in this computational model are caused by the interaction energy of the ions with the solvent, since this model does not explicitly consider hydrogen-bonding interactions, we show that their contribution is not required for such effects. However, these results should not be taken to mean that hydrogen-bonding

is not important for these property changes in real water and salt solutions. An important conclusion of studies aimed at understanding the impact of these high frequency fluctuations is that they give rise to a liquid having a remarkably high cohesive energy density.[124,125] This high cohesive energy density of water predominantly accounts for the relatively high boiling point, liquid-vapor critical temperature, T_c, melting point, T_m, surface tension, γ, and many other properties of this remarkable liquid.[124,125] This minimal CG model of water was constructed to be consistent with the high cohesive energy density of water, as the original formulation sought to recover the critical temperature of water,[33,34] a readily measured property of water that is well-known to be highly sensitive to the cohesive energy density.

Our successful comparison of simulation observations to QENS measurements of the collective relaxation time of aqueous salt solutions amplify on previous observations of the translational water self-diffusion coefficient, shear viscosity, surface tension, density, and isothermal compressibility of the same monovalent salt solutions.[33,34] Thus, the applicability of this model is certainly not restricted to the collective relaxation time of aqueous salt solutions. For every property considered so far, this model has been found to be in accord with measured relative properties of aqueous salt solutions over a wide range of salt concentrations. These results strongly support our original hypothesis that the previously unexplained specific ion effects on aqueous salt solution properties arise from how the additives influence the cohesive energy density of the fluid (shown in Figure S2a), and that the hydrogen bonding interactions are responsible for the remarkably high cohesive energy density of real water. We take the consistent performance of this CG model in reproducing essential trends in the properties of aqueous monovalent salt solutions examined so far to be highly encouraging. Of course, further tests of the model are clearly needed to establish its limitations.

In addition to finding agreement with the structural relaxation time of QENS measurements, this work provided additional insights into differences between kosmotropic and chaotropic ions. The virial *B*-coefficients, whose sign defines the existence of kosmotropic or chaotropic ions, respectively, were shown to be consistent for the shear viscosity, water diffusion coefficient, structural relaxation time, infinite-frequency shear viscosity, and the inverse Debye-Waller parameter, according to expectations from the Stokes-Einstein relation. Interestingly, some of these closely interrelated virials are amenable to analytic estimation within the frame of this CG model of salt solutions. We find that the magnitude of the *B*-coefficients of Na^+, K^+, and Cs^+ are linearly related to the difference between ion-solvent and solvent-solvent interaction parameters, $\epsilon_{i,w}$-$\epsilon_{w,w}$, and this scaling relation is derived from a simple analytic model of the structural relaxation time.

While many of these relaxation processes probed by different molecular dynamics simulation and measurement methods appear to be significantly influenced by added salt, it is hard to then formulate a

general theory relating to how the various reported alterations in hydrogen-bonding network dynamics allowing for the prediction of such changes. High frequency hydrogen-bonding measurements,[44–46] in particular, prompt the question of what constitutes the "structure" of the hydrogen-bonding network and how such a structure be measured. Since there appears to be no general consensus on this question, we find it difficult to make any meaningful test of the veracity of hydrogen-bonding structure breaking and making hypothesis with any confidence. We remark that first principal quantum-based simulations of aqueous salt solutions by Parrinello and coworkers[38], in which the electronic degrees of freedom are explicitly treated, confirmed the qualitative existence of chaotropic ions, but this work further reported no detectable change on the structure of the hydrogen-bonding network. Experimental studies probing the same high frequency hydrogen-bonding dynamics of water addressed in the first principal simulations, such as the work of Chen *et al*.[126] claim strong evidence for changes in hydrogen-bonding network based on a *mobility-based* metric of "structure". Other experimental studies of hydrogen bonding dynamics, such as the neutron scattering measurements, have focused more on relaxation processes occurring on a timescale on the order of a ps,[127] corresponding to a localization timescale.

If we assert that the local solution structure around additives in water is described in terms of such interfacial *mobility gradients* then we arrive at a measure that can inform on both local water mobility changes, as well as average mobility exhibited by the entire material. We explore the utility of the local mean square atomic displacement on the caging timescale, the Debye-Waller parameter of the solvent ($<u^2>$), as a structural metric describing local variations in water mobility, a computational construct that allows us to visualize the hydration layer around ions and which can visualization of mobility fluctuations at a molecular length scale.[47–52,109,110] This aligns with the localization timescale identified in neutron scattering measurements of water.[127] This qualitative structural picture of the hydration layer of ions is ironically quite reminiscent of the classical Frank-Wen model of ion hydration,[128] except that the structural parameter is a density-based definition of structure rather than a dynamic structural parameter we utilize in this work. Our simulations thus lead to a picture of ion solvation that preserves the general spirit of their intuitive model of ion hydration. An effect of this kind is also evident in previous CG studies of polymer nanocomposites,[47,118,119] and atomistic studies of water-soluble polymers[123,124]. The formation of interfacial layers of altered mobility when putting one substance into another is evidently *a more general phenomenon* than the formation of dynamic hydration layers around ions, polymers, or particles in water, and it would be of interest to better understand what factors control the widths of these dynamic interfacial layers and the intensity of the changes in the local mobility within them. The direct visualization of the dynamic hydration layer around ions in Figure 5 illustrates the mobility gradient generated by this methodology. There is compelling evidence that the difference in the interaction strength between water and either non-polar molecules or particles is also central to understanding *hydrophobic* interactions in water.[129,130] It would

be interesting in the future to explore the capacity of this CG aqueous solution model to rationalize this type of interaction, which is also commonly attributed specifically to an additive species disruption of water's hydrogen-bonding network. . We expect that our capacity to visualize the dynamic hydration layers derived from MD computation will provide important insights into the nature of hydration layers of proteins and other biopolymers in which the local structure of the molecules involves variable chemistry.

Lastly, we must recognize that the LJ model is overly simplified in accounting for multipolar interactions and polarizability effects characteristic of water molecules. However, the fact that the current model has already shown a currently unique ability to capture chaotropic behavior, while even the most advanced atomistic MD models, as currently formulated, cannot,[35] points to some minimal aspect is lacking in how ions influence the solution properties of these more atomistic water models. It would be straightforward to extend the current water model to the Stockmayer fluid,[131] which involves a superposition of the LJ potential and a point dipole interaction. This allows for precise estimates of the Boyle temperature where the second virial vanishes and the estimation of the critical temperature T_c.[132] This feature in a CG model would reproduce the critical temperature of water and allow the calculation of the dielectric constant of water and even gradients of the dielectric constant. At a more sophisticated level, it should also be possible for more complex water models, such as the popular and successful TIP4P/2005 water model,[133] which involves a LJ center, with three fixed point charges to capture the directional interactions of water. However, we think it is prudent to subject this simple CG model to further tests before moving on to these more advanced models of water. The temperature transferability in CG simulations should be considered, and the energy renormalization method may then be applied,[134–136] if a suitable atomistic ion model was available, which does not yet exist. We also expect that the fundamental relationships between ion-solvent and solvent-solvent interaction energies and the propagating effect on solvent mobility will prove to be revealing in understanding the ultimate basis of success for our simulations.

Supplementary Material

See the supplementary material for the ratio of viscosity and collective relaxation times, where each value is scaled by the respective property for pure solvent. The stress autocorrelation function was fit to three timescales and compared to the salt-dependent trends of other characteristic time values, with a discussion on the topic of time-salt superposition. We also show that the difference between the primary peak height for the cation-solvent RDF and the water-water RDF varies nearly linearly with the difference between the LJ interaction well depth parameters, $\epsilon_{iS} - \epsilon_{SS}$, and the corresponding ion B coefficients to a good approximation. The definition of the caging relaxation time used to define the Debye-Waller parameter is illustrated in Figure S4. The total Debye-Waller parameter radially averaged from the ion

surface in dilute solution was plotted with its normal and tangential components. Lastly, the probability distribution of a solvent bead being in a certain hydration layer shows that much of the solvent is close to added ions and the fraction of static hydration layer solvent in the largest percolated cluster shows complete percolation at 0.5 mol/L. A table of the pure solvent properties has been provided.

Acknowledgments

Computer time was provided by the National Institute of Standards and Technology (NIST). J.A.C. acknowledges partial support from the National Research Council-NIST Postdoctoral Fellowship Program. A special thank you to Alexandros Chremos for useful discussions and validation of computed $F_C(t)$ results. We thank Antonio Faraone for providing QENS measurement data and Wengang Zhang for algorithmic suggestions. We acknowledge useful conversations with Dr. Antonio Faraone of the Center for Neutron Research at NIST (Gaithersburg) for helpful conversations, and, in particular, bringing the interesting paper by Corridoni *et al*.[8] to our attention.

Notes

Certain commercial equipment, instruments, or materials are identified in this paper to foster understanding. Such identification does not imply recommendation or endorsement by the National Institute of Standards and Technology, nor does it imply that the materials or equipment identified are necessarily the best available for the purpose.

Author Declarations

The authors declare no conflict of interest.

References

(1) Marcus, Y. Effect of Ions on the Structure of Water: Structure Making and Breaking. *Chem. Rev.* **2009**, *109* (3), 1346–1370. https://doi.org/10.1021/cr8003828.

(2) Ben Ishai, P.; Mamontov, E.; Nickels, J. D.; Sokolov, A. P. Influence of Ions on Water Diffusion—A Neutron Scattering Study. *J. Phys. Chem. B* **2013**, *117* (25), 7724–7728. https://doi.org/10.1021/jp4030415.

(3) Sutera, S. P.; Skalak, R. The History of Poiseuille's Law. *Annu. Rev. Fluid Mech.* **1993**, *25* (1), 1–20. https://doi.org/10.1146/annurev.fl.25.010193.000245.

(4) Gregory, K. P.; Elliott, G. R.; Robertson, H.; Kumar, A.; Wanless, E. J.; Webber, G. B.; Craig, V. S. J.; Andersson, G. G.; Page, A. J. Understanding Specific Ion Effects and the Hofmeister Series. *Phys. Chem. Chem. Phys.* **2022**, *24* (21), 12682–12718. https://doi.org/10.1039/D2CP00847E.

(5) Collins, K. D.; Washabaugh, M. W. The Hofmeister Effect and the Behaviour of Water at Interfaces. *Q. Rev. Biophys.* **1985**, *18* (4), 323–422. https://doi.org/10.1017/S0033583500005369.

(6) Cox, W. M.; Wolfenden, J. H.; Hartley, H. B. The Viscosity of Strong Electrolytes Measured by a Differential Method. *Proc. R. Soc. Lond. Ser. Contain. Pap. Math. Phys. Character* **1997**, *145* (855), 475–488. https://doi.org/10.1098/rspa.1934.0113.

(7) Gurney, R. W. (Ronald W. *Ionic Processes in Solution.*; International chemical series; McGraw-Hill: New York, 1953.

(8) Corridoni, T.; Mancinelli, R.; Ricci, M. A.; Bruni, F. Viscosity of Aqueous Solutions and Local Microscopic Structure. *J. Phys. Chem. B* **2011**, *115* (48), 14008–14013. https://doi.org/10.1021/jp202755u.

(9) Mallamace, F.; Corsaro, C.; Stanley, H. E. A Singular Thermodynamically Consistent Temperature at the Origin of the Anomalous Behavior of Liquid Water. *Sci. Rep.* **2012**, *2* (1), 993. https://doi.org/10.1038/srep00993.

(10) Ludwig, R. Water: From Clusters to the Bulk. *Angew. Chem. Int. Ed.* **2001**, *40* (10), 1808–1827. https://doi.org/10.1002/1521-3773(20010518)40:10<1808::AID-ANIE1808>3.0.CO;2-1.

(11) Mishchuk, N. A.; Goncharuk, V. V. Anomalous Thermal Properties of Water. *J. Water Chem. Technol.* **2017**, *39* (6), 331–338. https://doi.org/10.3103/S1063455X17060042.

(12) Pickett, P. D.; Ma, Y.; Posey, N. D.; Lueckheide, M.; Prabhu, V. M. Structure and Phase Behavior of Polyampholytes and Polyzwitterions. In *Macromolecular Engineering*; Hadjichristidis, N., Gnanou, Y., Matyjaszewski, K., Muthukumar, M., Eds.; Wiley, 2022; pp 1–51. https://doi.org/10.1002/9783527815562.mme0056.

(13) Umapathi, R.; Reddy, P. M.; Rani, A.; Venkatesu, P. Influence of Additives on Thermoresponsive Polymers in Aqueous Media: A Case Study of Poly(*N* -Isopropylacrylamide). *Phys. Chem. Chem. Phys.* **2018**, *20* (15), 9717–9744. https://doi.org/10.1039/C7CP08172C.

(14) Ju, B.; Cao, S.; Zhang, S. Effect of Additives on the Cloud Point Temperature of 2-Hydroxy-3-Isopropoxypropyl Starch Solutions. *J. Phys. Chem. B* **2013**, *117* (39), 11830–11835. https://doi.org/10.1021/jp404083r.

(15) Kang, B.; Tang, H.; Zhao, Z.; Song, S. Hofmeister Series: Insights of Ion Specificity from Amphiphilic Assembly and Interface Property. *ACS Omega* **2020**, *5* (12), 6229–6239. https://doi.org/10.1021/acsomega.0c00237.

(16) Habuchi, S.; Kim, H.-B.; Kitamura, N. Water Structures in Ion-Exchange Resin Particles: Solvation Dynamics of Nile Blue A. *Anal. Chem.* **2001**, *73* (2), 366–372. https://doi.org/10.1021/ac0007276.

(17) Salis, A.; Ninham, B. W. Models and Mechanisms of Hofmeister Effects in Electrolyte Solutions, and Colloid and Protein Systems Revisited. *Chem Soc Rev* **2014**, *43* (21), 7358–7377. https://doi.org/10.1039/C4CS00144C.

(18) Cacace, M. G.; Landau, E. M.; Ramsden, J. J. The Hofmeister Series: Salt and Solvent Effects on Interfacial Phenomena. *Q. Rev. Biophys.* **1997**, *30* (3), 241–277. https://doi.org/10.1017/S0033583597003363.

(19) Parsons, D. F.; Boström, M.; Nostro, P. L.; Ninham, B. W. Hofmeister Effects: Interplay of Hydration, Nonelectrostatic Potentials, and Ion Size. *Phys. Chem. Chem. Phys.* **2011**, *13* (27), 12352. https://doi.org/10.1039/c1cp20538b.

(20) Jungwirth, P.; Tobias, D. J. Specific Ion Effects at the Air/Water Interface. *Chem. Rev.* **2006**, *106* (4), 1259–1281. https://doi.org/10.1021/cr0403741.

(21) Wei, W. Hofmeister Effects Shine in Nanoscience. *Adv. Sci.* **2023**, *10* (22), 2302057. https://doi.org/10.1002/advs.202302057.

(22) Leberman, R.; Soper, A. K. Effect of High Salt Concentrations on Water Structure. *Nature* **1995**, *378*, 364–366. https://doi.org/10.1038/378364a0.

(23) Mancinelli, R.; Botti, A.; Bruni, F.; Ricci, M. A.; Soper, A. K. Perturbation of Water Structure Due to Monovalent Ions in Solution. *Phys. Chem. Chem. Phys.* **2007**, *9* (23), 2959. https://doi.org/10.1039/b701855j.

(24) Mancinelli, R.; Botti, A.; Bruni, F.; Ricci, M. A.; Soper, A. K. Hydration of Sodium, Potassium, and Chloride Ions in Solution and the Concept of Structure Maker/Breaker. *J. Phys. Chem. B* **2007**, *111* (48), 13570–13577. https://doi.org/10.1021/jp075913v.

(25) Omta, A. W.; Kropman, M. F.; Woutersen, S.; Bakker, H. J. Negligible Effect of Ions on the Hydrogen-Bond Structure in Liquid Water. *Science* **2003**, *301* (5631), 347–349. https://doi.org/10.1126/science.1084801.

(26) Zhang, C.; Yue, S.; Panagiotopoulos, A. Z.; Klein, M. L.; Wu, X. Dissolving Salt Is Not Equivalent to Applying a Pressure on Water. *Nat. Commun.* **2022**, *13* (1), 822. https://doi.org/10.1038/s41467-022-28538-8.

(27) Luo, P.; Zhai, Y.; Senses, E.; Mamontov, E.; Xu, G.; Z, Y.; Faraone, A. Influence of Kosmotrope and Chaotrope Salts on Water Structural Relaxation. *J. Phys. Chem. Lett.* **2020**, *11* (21), 8970–8975. https://doi.org/10.1021/acs.jpclett.0c02619.

(28) Rezaei-Ghaleh, N. Water Dynamics in Highly Concentrated Salt Solutions: A Multi-Nuclear NMR Approach. *ChemistryOpen* **2022**, *11* (6), e202200080. https://doi.org/10.1002/open.202200080.

(29) Ball, P.; Hallsworth, J. E. Water Structure and Chaotropicity: Their Uses, Abuses and Biological Implications. *Phys. Chem. Chem. Phys.* **2015**, *17* (13), 8297–8305. https://doi.org/10.1039/C4CP04564E.

(30) Honig, B.; Sharp, K.; Yang, A. S. Macroscopic Models of Aqueous Solutions: Biological and Chemical Applications. *J. Phys. Chem.* **1993**, *97* (6), 1101–1109. https://doi.org/10.1021/j100108a002.

(31) Marcus, Y. The Structuredness of Water at Elevated Temperatures along the Saturation Line. *J. Mol. Liq.* **1999**, *79* (2), 151–165. https://doi.org/10.1016/S0167-7322(98)00109-3.

(32) Traube, J. The Attraction Pressure. *J. Phys. Chem.* **1910**, *14* (5), 452–470. https://doi.org/10.1021/j150113a003.

(33) Andreev, M.; Chremos, A.; de Pablo, J.; Douglas, J. F. Coarse-Grained Model of the Dynamics of Electrolyte Solutions. *J. Phys. Chem. B* **2017**, *121* (34), 8195–8202. https://doi.org/10.1021/acs.jpcb.7b04297.

(34) Andreev, M.; de Pablo, J. J.; Chremos, A.; Douglas, J. F. Influence of Ion Solvation on the Properties of Electrolyte Solutions. *J. Phys. Chem. B* **2018**, *122* (14), 4029–4034. https://doi.org/10.1021/acs.jpcb.8b00518.

(35) Panagiotopoulos, A. Z. Simulations of Activities, Solubilities, Transport Properties, and Nucleation Rates for Aqueous Electrolyte Solutions. *J. Chem. Phys.* **2020**, *153* (1), 010903. https://doi.org/10.1063/5.0012102.

(36) Kann, Z. R.; Skinner, J. L. A Scaled-Ionic-Charge Simulation Model That Reproduces Enhanced and Suppressed Water Diffusion in Aqueous Salt Solutions. *J. Chem. Phys.* **2014**, *141* (10), 104507. https://doi.org/10.1063/1.4894500.

(37) Kim, J. S.; Wu, Z.; Morrow, A. R.; Yethiraj, A.; Yethiraj, A. Self-Diffusion and Viscosity in Electrolyte Solutions. *J. Phys. Chem. B* **2012**, *116* (39), 12007–12013. https://doi.org/10.1021/jp306847t.

(38) Ding, Y.; Hassanali, A. A.; Parrinello, M. Anomalous Water Diffusion in Salt Solutions. *Proc. Natl. Acad. Sci.* **2014**, *111* (9), 3310–3315. https://doi.org/10.1073/pnas.1400675111.

(39) Yao, Y.; Kanai, Y.; Berkowitz, M. L. Role of Charge Transfer in Water Diffusivity in Aqueous Ionic Solutions. *J. Phys. Chem. Lett.* **2014**, *5* (15), 2711–2716. https://doi.org/10.1021/jz501238v.

(40) Panagiotopoulos, A. Z.; Yue, S. Dynamics of Aqueous Electrolyte Solutions: Challenges for Simulations. *J. Phys. Chem. B* **2023**, *127* (2), 430–437. https://doi.org/10.1021/acs.jpcb.2c07477.

(41) Zeron, I. M.; Abascal, J. L. F.; Vega, C. A Force Field of Li^+, Na^+, K^+, Mg^{2+}, Ca^{2+}, Cl^-, and $SO4^{2-}$ in Aqueous Solution Based on the TIP4P/2005 Water Model and Scaled Charges for the Ions. *J. Chem. Phys.* **2019**, *151* (13), 134504. https://doi.org/10.1063/1.5121392.

(42) Nguyen, M.; Rick, S. W. The Influence of Polarizability and Charge Transfer on Specific Ion Effects in the Dynamics of Aqueous Salt Solutions. *J. Chem. Phys.* **2018**, *148* (22), 222803. https://doi.org/10.1063/1.5012682.

(43) Mo, Y.; Gao, J. Polarization and Charge-Transfer Effects in Aqueous Solution via Ab Initio QM/MM Simulations. *J. Phys. Chem. B* **2006**, *110* (7), 2976–2980. https://doi.org/10.1021/jp057017u.

(44) González-Jiménez, M.; Liao, Z.; Williams, E. L.; Wynne, K. Lifting Hofmeister's Curse: Impact of Cations on Diffusion, Hydrogen Bonding, and Clustering of Water. *J. Am. Chem. Soc.* **2024**, *146* (1), 368–376. https://doi.org/10.1021/jacs.3c09421.

(45) Heisler, I. A.; Meech, S. R. Low-Frequency Modes of Aqueous Alkali Halide Solutions: Glimpsing the Hydrogen Bonding Vibration. *Science* **2010**, *327* (5967), 857–860. https://doi.org/10.1126/science.1183799.

(46) Singh, A. K.; Doan, L. C.; Lou, D.; Wen, C.; Vinh, N. Q. Interfacial Layers between Ion and Water Detected by Terahertz Spectroscopy. *J. Chem. Phys.* **2022**, *157* (5), 054501. https://doi.org/10.1063/5.0095932.

(47) Zhu, Y.; Giuntoli, A.; Zhang, W.; Lin, Z.; Keten, S.; Starr, F. W.; Douglas, J. F. The Effect of Nanoparticle Softness on the Interfacial Dynamics of a Model Polymer Nanocomposite. *J. Chem. Phys.* **2022**, *157* (9), 094901. https://doi.org/10.1063/5.0101551.

(48) Horstmann, R.; Vogel, M. Common Behaviors Associated with the Glass Transitions of Water-like Models. *J. Chem. Phys.* **2017**, *147* (3), 034505. https://doi.org/10.1063/1.4993445.

(49) Haddadian, E. J.; Zhang, H.; Freed, K. F.; Douglas, J. F. Comparative Study of the Collective Dynamics of Proteins and Inorganic Nanoparticles. *Sci. Rep.* **2017**, *7* (1), 41671. https://doi.org/10.1038/srep41671.

(50) Clark, J. A.; Prabhu, V. M.; Douglas, J. F. Molecular Dynamics Simulation of the Influence of Temperature and Salt on the Dynamic Hydration Layer in a Model Polyzwitterionic Polymer PAEDAPS. *J. Phys. Chem. B* **2023**, *127* (38), 8185–8198. https://doi.org/10.1021/acs.jpcb.3c03654.

(51) Larini, L.; Ottochian, A.; De Michele, C.; Leporini, D. Universal Scaling between Structural Relaxation and Vibrational Dynamics in Glass-Forming Liquids and Polymers. *Nat. Phys.* **2008**, *4* (1), 42–45. https://doi.org/10.1038/nphys788.

(52) Starr, F. W.; Sastry, S.; Douglas, J. F.; Glotzer, S. C. What Do We Learn from the Local Geometry of Glass-Forming Liquids? *Phys. Rev. Lett.* **2002**, *89* (12), 125501. https://doi.org/10.1103/PhysRevLett.89.125501.

(53) Klein, C.; Sallai, J.; Jones, T. J.; Iacovella, C. R.; McCabe, C.; Cummings, P. T. A Hierarchical, Component Based Approach to Screening Properties of Soft Matter. In *Foundations of Molecular*

Modeling and Simulation; Snurr, R. Q., Adjiman, C. S., Kofke, D. A., Eds.; Molecular Modeling and Simulation; Springer Singapore: Singapore, 2016; pp 79–92. https://doi.org/10.1007/978-981-10-1128-3_5.

(54) Klein, C.; Summers, A. Z.; Thompson, M. W.; Gilmer, J. B.; McCabe, C.; Cummings, P. T.; Sallai, J.; Iacovella, C. R. Formalizing Atom-Typing and the Dissemination of Force Fields with Foyer. *Comput. Mater. Sci.* **2019**, *167*, 215–227. https://doi.org/10.1016/j.commatsci.2019.05.026.

(55) Collins, K. D. The Behavior of Ions in Water Is Controlled by Their Water Affinity. *Q. Rev. Biophys.* **2019**, *52*, e11. https://doi.org/10.1017/S0033583519000106.

(56) Jenkins, H. D. B.; Marcus, Y. Viscosity B-Coefficients of Ions in Solution. *Chem. Rev.* **1995**, *95*, 2695–2724. https://doi.org/10.1021/cr00040a004.

(57) Capponi, S.; White, S. H.; Tobias, D. J.; Heyden, M. Structural Relaxation Processes and Collective Dynamics of Water in Biomolecular Environments. *J. Phys. Chem. B* **2019**, *123* (2), 480–486. https://doi.org/10.1021/acs.jpcb.8b12052.

(58) Thompson, A. P.; Aktulga, H. M.; Berger, R.; Bolintineanu, D. S.; Brown, W. M.; Crozier, P. S.; in 't Veld, P. J.; Kohlmeyer, A.; Moore, S. G.; Nguyen, T. D.; et al. LAMMPS - a Flexible Simulation Tool for Particle-Based Materials Modeling at the Atomic, Meso, and Continuum Scales. *Comput. Phys. Commun.* **2022**, *271*, 108171. https://doi.org/10.1016/j.cpc.2021.108171.

(59) Hockney, R. W.; Eastwood, J. W. *Computer Simulation Using Particles*, 0 ed.; CRC Press, 2021. https://doi.org/10.1201/9780367806934.

(60) Maginn, E. J.; Messerly, R. A.; Carlson, D. J.; Roe, D. R.; Elliot, J. R. Best Practices for Computing Transport Properties 1. Self-Diffusivity and Viscosity from Equilibrium Molecular Dynamics [Article v1.0]. *Living J. Comput. Mol. Sci.* **2020**, *1* (1), 6324. https://doi.org/10.33011/livecoms.1.1.6324.

(61) Basconi, J. E.; Shirts, M. R. Effects of Temperature Control Algorithms on Transport Properties and Kinetics in Molecular Dynamics Simulations. *J. Chem. Theory Comput.* **2013**, *9* (7), 2887–2899. https://doi.org/10.1021/ct400109a.

(62) Gowers, R.; Linke, M.; Barnoud, J.; Reddy, T.; Melo, M.; Seyler, S.; Domański, J.; Dotson, D.; Buchoux, S.; Kenney, I.; et al. MDAnalysis: A Python Package for the Rapid Analysis of Molecular Dynamics Simulations; Austin, Texas, 2016; pp 98–105. https://doi.org/10.25080/Majora-629e541a-00e.

(63) Michaud-Agrawal, N.; Denning, E. J.; Woolf, T. B.; Beckstein, O. MDAnalysis: A Toolkit for the Analysis of Molecular Dynamics Simulations. *J. Comput. Chem.* **2011**, *32* (10), 2319–2327. https://doi.org/10.1002/jcc.21787.

(64) Enderby, J. E. Neutron Diffraction, Isotopic Substitution and the Structure of Aqueous Solutions. *Philos. Trans. R. Soc. Lond. B. Biol. Sci.* **1980**, *290*, 553–566. https://doi.org/10.1098/rstb.1980.0115.

(65) Mason, P. E.; Ansell, S.; Neilson, G. W.; Rempe, S. B. Neutron Scattering Studies of the Hydration Structure of Li^+. *J. Phys. Chem. B* **2015**, *119* (5), 2003–2009. https://doi.org/10.1021/jp511508n.

(66) Cummings, S.; Enderby, J. E.; Neilson, G. W.; Newsome, J. R.; Howe, R. A.; Howells, W. S.; Soper, A. K. Chloride Ions in Aqueous Solutions. *Nature* **1980**, *287* (5784), 714–716. https://doi.org/10.1038/287714a0.

(67) Teixeira, J.; Bellissent-Funel, M.-C.; Chen, S. H.; Dianoux, A. J. Experimental Determination of the Nature of Diffusive Motions of Water Molecules at Low Temperatures. *Phys. Rev. A* **1985**, *31* (3), 1913–1917. https://doi.org/10.1103/PhysRevA.31.1913.

(68) Teixeira, J.; Luzar, A.; Longeville, S. Dynamics of Hydrogen Bonds: How to Probe Their Role in the Unusual Properties of Liquid Water. *J. Phys. Condens. Matter* **2006**, *18* (36), S2353–S2362. https://doi.org/10.1088/0953-8984/18/36/S09.

(69) Salacuse, J. J.; Denton, A. R.; Egelstaff, P. A. Finite-Size Effects in Molecular Dynamics Simulations: Static Structure Factor and Compressibility. I. Theoretical Method. *Phys. Rev. E* **1996**, *53* (3), 2382–2389. https://doi.org/10.1103/PhysRevE.53.2382.

(70) Salacuse, J. J.; Denton, A. R.; Egelstaff, P. A.; Tau, M.; Reatto, L. Finite-Size Effects in Molecular Dynamics Simulations: Static Structure Factor and Compressibility. II. Application to a Model Krypton Fluid. *Phys. Rev. E* **1996**, *53* (3), 2390–2401. https://doi.org/10.1103/PhysRevE.53.2390.

(71) Salacuse, J. J.; Egelstaff, P. A. Finite-Size Effects in Molecular Dynamics Simulations: Intermediate Scattering Function and Velocity of Sound. III. Theory and Application to a Model Krypton Fluid. *Phys. Rev. E* **2001**, *64* (5), 051201. https://doi.org/10.1103/PhysRevE.64.051201.

(72) Arbe, A.; Nilsen, G. J.; Stewart, J. R.; Alvarez, F.; Sakai, V. G.; Colmenero, J. Coherent Structural Relaxation of Water from Meso- to Intermolecular Scales Measured Using Neutron Spectroscopy with Polarization Analysis. *Phys. Rev. Res.* **2020**, *2* (2), 022015. https://doi.org/10.1103/PhysRevResearch.2.022015.

(73) Starr, F. W.; Douglas, J. F.; Sastry, S. The Relationship of Dynamical Heterogeneity to the Adam-Gibbs and Random First-Order Transition Theories of Glass Formation. *J. Chem. Phys.* **2013**, *138* (12), 12A541. https://doi.org/10.1063/1.4790138.

(74) Xu, W.-S.; Douglas, J. F.; Xu, X. Molecular Dynamics Study of Glass Formation in Polymer Melts with Varying Chain Stiffness. *Macromolecules* **2020**, *53* (12), 4796–4809. https://doi.org/10.1021/acs.macromol.0c00731.

(75) Chen, S.-H.; Mallamace, F.; Mou, C.-Y.; Broccio, M.; Corsaro, C.; Faraone, A.; Liu, L. The Violation of the Stokes–Einstein Relation in Supercooled Water. *Proc. Natl. Acad. Sci.* **2006**, *103* (35), 12974–12978. https://doi.org/10.1073/pnas.0603253103.

(76) Kumar, P.; Buldyrev, S. V.; Becker, S. R.; Poole, P. H.; Starr, F. W.; Stanley, H. E. Relation between the Widom Line and the Breakdown of the Stokes–Einstein Relation in Supercooled Water. *Proc. Natl. Acad. Sci.* **2007**, *104* (23), 9575–9579. https://doi.org/10.1073_pnas.0702608104.

(77) Xu, L. Appearance of a Fractional Stokes-Einstein Relation in Water and a Structural Interpretation of Its Onset. *Nat. Phys.* **2009**, *5*, 565–569. https://doi.org/10.1038/nphys1328.

(78) Wu, B.; Iwashita, T.; Egami, T. Atomic Dynamics in Simple Liquid: De Gennes Narrowing Revisited. *Phys. Rev. Lett.* **2018**, *120* (13), 135502. https://doi.org/10.1103/PhysRevLett.120.135502.

(79) Iwashita, T.; Nicholson, D. M.; Egami, T. Elementary Excitations and Crossover Phenomenon in Liquids. *Phys. Rev. Lett.* **2013**, *110* (20), 205504. https://doi.org/10.1103/PhysRevLett.110.205504.

(80) Maxwell, J. C. IV. On the Dynamical Theory of Gases. *Philos. Trans. R. Soc. Lond.* **1867**, *157*, 49–88. https://doi.org/10.1098/rstl.1867.0004.

(81) Dyre, J. C.; Wang, W. H. The Instantaneous Shear Modulus in the Shoving Model. *J Chem Phys* **2021**, *136*, 224108. https://doi.org/10.1063/1.4724102.

(82) Zwanzig, R.; Mountain, R. High-Frequency Elastic Moduli of Simple Fluids. *J. Chem. Phys.* **1965**, *43*, 4464–4471. https://doi.org/10.1063/1.1696718.

(83) Sauer, B. B.; Dee, G. T. Surface Tension and Melt Cohesive Energy Density of Polymer Melts Including High Melting and High Glass Transition Polymers. *Macromolecules* **2002**, *35* (18), 7024–7030. https://doi.org/10.1021/ma0202437.

(84) Lee, S.; Goo Lee, J.; Lee, H.; Mumby, S. J. Molecular Dynamics Simulations of the Enthalpy of Mixing of Poly(Vinyl Chloride) and Aliphatic Polyester Blends. *Polymer* **1999**, *40* (18), 5137–5145. https://doi.org/10.1016/S0032-3861(98)00586-2.

(85) Ren, G.; Chen, L.; Wang, Y. Dynamic Heterogeneity in Aqueous Ionic Solutions. *Phys. Chem. Chem. Phys.* **2018**, *20* (33), 21313–21324. https://doi.org/10.1039/C8CP02787K.

(86) Shi, Z.; Debenedetti, P. G.; Stillinger, F. H. Relaxation Processes in Liquids: Variations on a Theme by Stokes and Einstein. *J. Chem. Phys.* **2013**, *138* (12), 12A526. https://doi.org/10.1063/1.4775741.

(87) Maranas, J. K.; Kumar, S. K.; Debenedetti, P. G.; Graessley, W. W.; Mondello, M.; Grest, G. S. Liquid Structure, Thermodynamics, and Mixing Behavior of Saturated Hydrocarbon Polymers. 2. Pair Distribution Functions and the Regularity of Mixing. *Macromolecules* **1998**, *31* (20), 6998–7002. https://doi.org/10.1021/ma971756u.

(88) Andrews, J.; Handler, R. A.; Blaisten-Barojas, E. Structure, Energetics and Thermodynamics of PLGA Condensed Phases from Molecular Dynamics. *Polymer* **2020**, *206*, 122903. https://doi.org/10.1016/j.polymer.2020.122903.

(89) Xu, W.-S.; Douglas, J. F.; Freed, K. F. Influence of Cohesive Energy on the Thermodynamic Properties of a Model Glass-Forming Polymer Melt. *Macromolecules* **2016**, *49* (21), 8341–8354. https://doi.org/10.1021/acs.macromol.6b01503.

(90) Levashov, V. A.; Morris, J. R.; Egami, T. The Origin of Viscosity as Seen through Atomic Level Stress Correlation Function. *J Chem Phys* **2013**, *138*, 044507. https://doi.org/10.1063/1.4789306.

(91) Ali, S.; Prabhu, V. M. Relaxation Behavior by Time-Salt and Time-Temperature Superpositions of Polyelectrolyte Complexes from Coacervate to Precipitate. *Gels* **2018**, *4* (1), 11. https://doi.org/10.3390/gels4010011.

(92) Heo, T.-Y.; Kim, S.; Chen, L.; Sokolova, A.; Lee, S.; Choi, S.-H. Molecular Exchange Kinetics in Complex Coacervate Core Micelles: Role of Associative Interaction. *ACS Macro Lett.* **2021**, *10*, 1138−1144. https://doi.org/10.1021/acsmacrolett.1c00482.

(93) Spruijt, E.; Sprakel, J.; Lemmers, M.; Stuart, M. A. C. Relaxation Dynamics at Different Time Scales in Electrostatic Complexes: Time-Salt Superposition. *Phys. Rev. Lett.* **2010**, *105*, 208301. https://doi.org/10.1103/PhysRevLett.105.208301.

(94) Jones, G.; Dole, M. The Viscosity of Aqueous Solutions of Strong Electrolytes with Special Reference to Barium Chloride. *J. Am. Chem. Soc.* **1929**, *51* (10), 2950–2964. https://doi.org/10.1021/ja01385a012.

(95) Debye, P.; Hückel, E. Zur Theorie Der Elektrolyte. I. Gefrierpunktserniedrigung Und Verwandte Erscheinungen. *Phys. Z.* **1923**, *24*, 185–206.

(96) Einstein, A. Über Die von Der Molekularkinetischen Theorie Der Wärme Geforderte Bewegung von in Ruhenden Flüssigkeiten Suspendierten Teilchen. *Ann. Phys.* **1905**, *322* (8), 549–560. https://doi.org/10.1002/andp.19053220806.

(97) Stokes, G. G. On the Effect of the Internal Friction of Fluids on the Motion of Pendulums. *Trans. Camb. Philos. Soc.* **1851**, *9*, 8–106. https://doi.org/10.1017/CBO9780511702266.002.

(98) Speedy, R. J.; Prielmeier, F. X.; Vardag, T.; Lang, E. W.; Lüdemann, H.-D. Diffusion in Simple Fluids. *Mol. Phys.* **1989**, *66* (3), 577–590. https://doi.org/10.1080/00268978900100341.

(99) Liu, H.; Silva, C. M.; Macedo, E. A. Unified Approach to the Self-Diffusion Coefficients of Dense Fluids over Wide Ranges of Temperature and Pressure—Hard-Sphere, Square-Well, Lennard–Jones and Real Substances. *Chem. Eng. Sci.* **1998**, *53* (13), 2403–2422. https://doi.org/10.1016/S0009-2509(98)00036-0.

(100) Chen, Q.; Tian, J. A Connection between the Density and Temperature of the Lennard-Jones Fluids at Equilibrium and the First Peak of the Radial Distribution Function. *Fluid Phase Equilibria* **2023**, *567*, 113709. https://doi.org/10.1016/j.fluid.2022.113709.

(101) Dyre, J. C.; Olsen, N. B. Landscape Equivalent of the Shoving Model. *Phys. Rev. E* **2004**, *69*, 042501. https://doi.org/10.1103/PhysRevE.69.042501.

(102) Dyre, J. C.; Olsen, N. B.; Christensen, T. Local Elastic Expansion Model for Viscous - FLow Activation Energies of Glass-Forming Molecular Liquids. *Phys. Rev. B* **1996**, *53*, 2172. https://doi.org/10.1103/PhysRevB.53.2171.

(103) Glasstone, S.; Laidler, K. J. (Keith J.; Eyring, H. *The Theory of Rate Processes; the Kinetics of Chemical Reactions, Viscosity, Diffusion and Electrochemical Phenomena*, First edition.; International chemical series; McGraw-Hill Book Company, inc.: New York;, 1941.

(104) Puosi, F.; Leporini, D. The Kinetic Fragility of Liquids as Manifestation of the Elastic Softening. *Eur. Phys. J. E* **2015**, *38* (8), 87. https://doi.org/10.1140/epje/i2015-15087-2.

(105) Simmons, D. S.; Cicerone, M. T.; Zhong, Q.; Tyagi, M.; Douglas, J. F. Generalized Localization Model of Relaxation in Glass-Forming Liquids. *Soft Matter* **2012**, *8* (45), 11455. https://doi.org/10.1039/c2sm26694f.

(106) Pazmiño Betancourt, B. A.; Hanakata, P. Z.; Starr, F. W.; Douglas, J. F. Quantitative Relations between Cooperative Motion, Emergent Elasticity, and Free Volume in Model Glass-Forming Polymer Materials. *Proc. Natl. Acad. Sci.* **2015**, *112* (10), 2966–2971. https://doi.org/10.1073/pnas.1418654112.

(107) Douglas, J. F.; Pazmino Betancourt, B. A.; Tong, X.; Zhang, H. Localization Model Description of Diffusion and Structural Relaxation in Glass-Forming Cu–Zr Alloys. *J. Stat. Mech. Theory Exp.* **2016**, *2016* (5), 054048. https://doi.org/10.1088/1742-5468/2016/05/054048.

(108) Mahmud, G.; Zhang, H.; Douglas, J. F. Localization Model Description of the Interfacial Dynamics of Crystalline Cu and Cu64Zr36 Metallic Glass Films. *J. Chem. Phys.* **2020**, *153* (12), 124508. https://doi.org/10.1063/5.0022937.

(109) Fichou, Y.; Schirò, G.; Gallat, F.-X.; Laguri, C.; Moulin, M.; Combet, J.; Zamponi, M.; Härtlein, M.; Picart, C.; Mossou, E.; et al. Hydration Water Mobility Is Enhanced around Tau Amyloid Fibers. *Proc. Natl. Acad. Sci.* **2015**, *112* (20), 6365–6370. https://doi.org/10.1073/pnas.1422824112.

(110) Zheng, X.; Guo, Y.; Douglas, J. F.; Xia, W. Understanding the Role of Cross-Link Density in the Segmental Dynamics and Elastic Properties of Cross-Linked Thermosets. *J. Chem. Phys.* **2022**, *157* (6), 064901. https://doi.org/10.1063/5.0099322.

(111) Psurek, T.; Soles, C. L.; Page, K. A.; Cicerone, M. T.; Douglas, J. F. Quantifying Changes in the High-Frequency Dynamics of Mixtures by Dielectric Spectroscopy. *J. Phys. Chem. B* **2008**, *112* (50), 15980–15990. https://doi.org/10.1021/jp8034314.

(112) Hartkamp, R.; Coasne, B. Structure and Transport of Aqueous Electrolytes: From Simple Halides to Radionuclide Ions. *J. Chem. Phys.* **2014**, *141* (12), 124508. https://doi.org/10.1063/1.4896380.

(113) Weitzner, S. E.; Pham, T. A.; Orme, C. A.; Qiu, S. R.; Wood, B. C. Beyond Thermodynamics: Assessing the Dynamical Softness of Hydrated Ions from First Principles. *J. Phys. Chem. Lett.* **2021**, *12* (49), 11980–11986. https://doi.org/10.1021/acs.jpclett.1c03314.

(114) Ohtaki, Hitoshi.; Radnai, Tamas. Structure and Dynamics of Hydrated Ions. *Chem. Rev.* **1993**, *93* (3), 1157–1204. https://doi.org/10.1021/cr00019a014.

(115) Wang, J. H. Effect of Ions on the Self-Diffusion and Structure of Water in Aqueous Electrolytic Solutions. *J. Phys. Chem.* **1954**, *58* (9), 686–692. https://doi.org/10.1021/j150519a003.

(116) Tobias, D. J.; Hemminger, J. C. Getting Specific About Specific Ion Effects. *Science* **2008**, *319* (5867), 1197–1198. https://doi.org/10.1126/science.1152799.

(117) Widom, B.; Ben-Amotz, D. Note on the Energy Density in the Solvent Induced by a Solute. *Proc. Natl. Acad. Sci.* **2006**, *103* (50), 18887–18890. https://doi.org/10.1073/pnas.0608996103.

(118) Zhang, W.; Douglas, J. F.; Starr, F. W. Effects of a "Bound" Substrate Layer on the Dynamics of Supported Polymer Films. *J. Chem. Phys.* **2017**, *147* (4), 044901. https://doi.org/10.1063/1.4994064.

(119) Zhang, W.; Emamy, H.; Pazmiño Betancourt, B. A.; Vargas-Lara, F.; Starr, F. W.; Douglas, J. F. The Interfacial Zone in Thin Polymer Films and around Nanoparticles in Polymer Nanocomposites. *J. Chem. Phys.* **2019**, *151* (12), 124705. https://doi.org/10.1063/1.5119269.

(120) Assaf, K. I.; Nau, W. M. The Chaotropic Effect as an Assembly Motif in Chemistry. *Angew. Chem. Int. Ed.* **2018**, *57* (43), 13968–13981. https://doi.org/10.1002/anie.201804597.

(121) Kabir, S. R.; Yokoyama, K.; Mihashi, K.; Kodama, T.; Suzuki, M. Hyper-Mobile Water Is Induced around Actin Filaments. *Biophys. J.* **2003**, *85* (5), 3154–3161. https://doi.org/10.1016/S0006-3495(03)74733-X.

(122) Elliott, J. A. W.; Prickett, R. C.; Elmoazzen, H. Y.; Porter, K. R.; McGann, L. E. A Multisolute Osmotic Virial Equation for Solutions of Interest in Biology. *J. Phys. Chem. B* **2007**, *111* (7), 1775–1785. https://doi.org/10.1021/jp0680342.

(123) Prickett, R. C.; Elliott, J. A. W.; McGann, L. E. Application of the Multisolute Osmotic Virial Equation to Solutions Containing Electrolytes. *J. Phys. Chem. B* **2011**, *115* (49), 14531–14543. https://doi.org/10.1021/jp206011m.

(124) Cabane, B.; Vuilleumier, R. The Physics of Liquid Water. *Comptes Rendus Geosci.* **2005**, *337* (1–2), 159–171. https://doi.org/10.1016/j.crte.2004.09.018.

(125) McGrath, M. J.; Kuo, I.-F. W.; Siepmann, J. I. Liquid Structures of Water, Methanol, and Hydrogen Fluoride at Ambient Conditions from First Principles Molecular Dynamics Simulations with a Dispersion Corrected Density Functional. *Phys. Chem. Chem. Phys.* **2011**, *13* (44), 19943. https://doi.org/10.1039/c1cp21890e.

(126) Chen, Y.; Okur, H. I.; Gomopoulos, N.; Macias-Romero, C.; Cremer, P. S.; Petersen, P. B.; Tocci, G.; Wilkins, D. M.; Liang, C.; Ceriotti, M.; et al. Electrolytes Induce Long-Range Orientational Order and Free Energy Changes in the H-Bond Network of Bulk Water. *Sci. Adv.* **2016**, *2* (4), e1501891. https://doi.org/10.1126/sciadv.1501891.

(127) Arbe, A.; Malo De Molina, P.; Alvarez, F.; Frick, B.; Colmenero, J. Dielectric Susceptibility of Liquid Water: Microscopic Insights from Coherent and Incoherent Neutron Scattering. *Phys. Rev. Lett.* **2016**, *117* (18), 185501. https://doi.org/10.1103/PhysRevLett.117.185501.

(128) Frank, H. S.; Wen, W.-Y. Ion-Solvent Interaction. Structural Aspects of Ion-Solvent Interaction in Aqueous Solutions: A Suggested Picture of Water Structure. *Discuss Faraday Soc* **1957**, *24*, 133–140. https://doi.org/10.1039/DF9572400133.

(129) Lazaridis, T. Solvent Size vs Cohesive Energy as the Origin of Hydrophobicity. *Acc. Chem. Res.* **2001**, *34* (12), 931–937. https://doi.org/10.1021/ar010058y.

(130) Otto, S. The Role of Solvent Cohesion in Nonpolar Solvation. *Chem. Sci.* **2013**, *4*, 2953. https://doi.org/10.1039/c3sc50740h.

(131) Stockmayer, W. H. Second Virial Coefficients of Polar Gases. *J. Chem. Phys.* **1941**, *9* (5), 398–402. https://doi.org/10.1063/1.1750922.

(132) Dudowicz, J.; Freed, K. F.; Douglas, J. F. Flory-Huggins Model of Equilibrium Polymerization and Phase Separation in the Stockmayer Fluid. *Phys. Rev. Lett.* **2004**, *92* (4), 045502. https://doi.org/10.1103/PhysRevLett.92.045502.

(133) Abascal, J. L. F.; Vega, C. A General Purpose Model for the Condensed Phases of Water: TIP4P/2005. *J. Chem. Phys.* **2005**, *123* (23), 234505. https://doi.org/10.1063/1.2121687.

(134) Xia, W.; Song, J.; Hansoge, N. K.; Phelan, F. R.; Keten, S.; Douglas, J. F. Energy Renormalization for Coarse-Graining the Dynamics of a Model Glass-Forming Liquid. *J. Phys. Chem. B* **2018**, *122* (6), 2040–2045. https://doi.org/10.1021/acs.jpcb.8b00321.

(135) Xia, W.; Song, J.; Jeong, C.; Hsu, D. D.; Phelan, F. R.; Douglas, J. F.; Keten, S. Energy-Renormalization for Achieving Temperature Transferable Coarse-Graining of Polymer Dynamics. *Macromolecules* **2017**, *50* (21), 8787–8796. https://doi.org/10.1021/acs.macromol.7b01717.

(136) Xia, W.; Hansoge, N. K.; Xu, W.-S.; Phelan, F. R.; Keten, S.; Douglas, J. F. Energy Renormalization for Coarse-Graining Polymers Having Different Segmental Structures. *Sci. Adv.* **2019**, *5* (4), eaav4683. https://doi.org/10.1126/sciadv.aav4683.

TOC Graphic

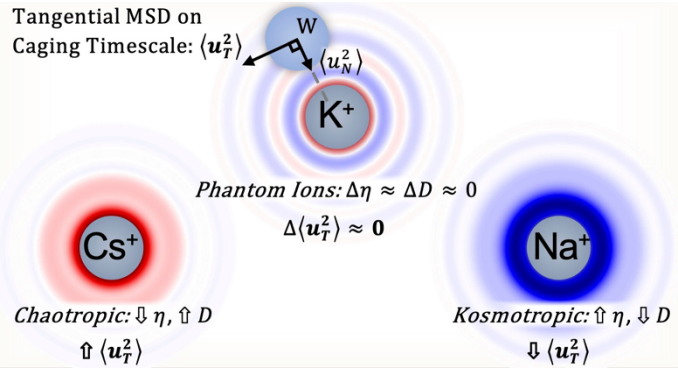
Tangential MSD on
Caging Timescale: $\langle u_T^2 \rangle$
W
$\langle u_N^2 \rangle$
K+
Phantom Ions: $\Delta\eta \approx \Delta D \approx 0$
$\Delta\langle u_T^2 \rangle \approx 0$
Cs+
Na+
Chaotropic: $\Downarrow \eta, \Uparrow D$
$\Uparrow \langle u_T^2 \rangle$
Kosmotropic: $\Uparrow \eta, \Downarrow D$
$\Downarrow \langle u_T^2 \rangle$